European Journal of Medicinal Chemistry 263 (2024) 115951

Contents lists available at ScienceDirect

European Journal of Medicinal Chemistry

journal homepage: www.elsevier.com/locate/ejmech

Research paper

Unexpected rearrangement of ivermectin in the synthesis of new derivatives with trypanocidal and antiplasmodial activities

Michał Sulik [a], Diana Fontinha [b], Dietmar Steverding [c], Szymon Sobczak [d], Michał Antoszczak [a], Miguel Prudêncio [b], Adam Huczyński [a,*]

[a] Department of Medical Chemistry, Faculty of Chemistry, Adam Mickiewicz University, Uniwersytetu Poznańskiego 8, 61–614 Poznań, Poland
[b] Instituto de Medicina Molecular João Lobo Antunes, Faculdade de Medicina, Universidade de Lisboa, Av. Prof. Egas Moniz, 1649-028, Lisboa, Portugal
[c] Bob Champion Research & Education Building, Norwich Medical School, University of East Anglia, Norwich, UK
[d] Department of Materials Chemistry, Faculty of Chemistry, Adam Mickiewicz University, Uniwersytetu Poznańskiego 8, 61–614 Poznań, Poland

ARTICLE INFO

Handling Editor: Dr. Z Liu

Keywords:
Ivermectin
C13-*epi*-amide derivatives
Trypanosoma brucei
Trypanocidal activity
Plasmodium berghei
Plasmodicidal activity

ABSTRACT

Ivermectin is a sixteen-membered macrolactone "wonder drug" of Nobel prize-honored distinction that exhibits a wide range of antiparasitic activities. It has been used for almost four decades in the treatment of various parasitic diseases in humans and animals. In this paper, we describe the synthesis of the first-in-class ivermectin derivatives obtained via derivatization of the C13 position, along with the unexpected rearrangement of the oxahydrindene (hexahydrobenzofuran) unit of the macrolide ring. The structural investigation of the rearrangement has been performed using the single-crystal X-ray diffraction method. The antiparasitic and cytotoxic activities of the newly synthesized derivatives were determined *in vitro* with the bloodstream form of *Trypanosoma brucei brucei*, the hepatic stage of *Plasmodium berghei*, and human leukemia HL-60 cells. The compounds with the highest trypanocidal activity were the C13-*epi*-2-chloroacetamide analogs of native (**6h**) or rearranged (**7h**) ivermectin. Both **6h** and **7h** displayed trypanocidal activities within a similar mid-nanomolar concentration range as the commercially used trypanocides suramin and ethidium bromide. Furthermore, **6h** and **7h** exhibited a comparable cytotoxic to trypanocidal ratio as the reference drug ethidium bromide. The double-modified compound **7a** (C13-*epi*-acetamide of rearranged ivermectin) exhibited the highest activity against *P. berghei* grown in human hepatoma cells, which was 2.5 times higher than that of ivermectin. The findings of this study suggest that C13-*epi*-amide derivatives of ivermectin are suitable leads in the rational development of new antiparasitic agents.

1. Introduction

Ivermectin (**IVR**, **1**, Fig. 1) is a sixteen-membered macrolactone and the C22,C23-dihydro derivative of avermectin (Fig. 1), which was first isolated from a *Streptomyces avermitilis* strain in Japan in 1967 [1]. A broad range of antiparasitic activities of **IVR**, combined with its safe use, has led to numerous applications of the drug in the treatment of several parasitic diseases, including river blindness and elephantiasis [2,3]. Mechanistically, **IVR** potentiates the glutamate-gated chloride ion channels (GluCl), resulting in the hyperpolarization of parasite muscles and nerves [3]. Moreover, **IVR** has the ability to inhibit the conductance of γ-aminobutyric acid (GABA) channels, while in the asexual blood stages of *Plasmodium falciparum*, the drug has been found to inhibit importin (IMP) α/β, a heterodimer that transports proteins to the nucleus across the nuclear complex pore [3]. **IVR** has significantly influenced medical treatments that many scientists call it a "wonder drug" [4], and its discovery, together with that of artemisinin as antimalarial drug, was awarded the Nobel Prize in Physiology/Medicine in 2015 [5]. **IVR** is used in human and veterinary medicine as a mixture of two forms – B1a with an ethyl group at the C26 position, and B1b with a methyl group at this position (Fig. 1) [6]. The mixture consists of at least 80 % of **IVR** B1a and a maximum of 20 % of **IVR** B1b [6].

Neglected tropical diseases (NTDs) are a group of about 20 different infections that mainly affect people living in poverty in tropical and subtropical regions [7]. It is estimated that NTDs are a health and economic threat to approximately one billion people worldwide [7]. However, many NTDs could be easily and cost-effectively controlled, as preventive measures are relatively cheap and bring an estimated benefit

* Corresponding author.
E-mail address: adhucz@amu.edu.pl (A. Huczyński).

https://doi.org/10.1016/j.ejmech.2023.115951
Received 6 October 2023; Received in revised form 8 November 2023; Accepted 9 November 2023
Available online 16 November 2023
0223-5234/© 2023 The Authors. Published by Elsevier Masson SAS. This is an open access article under the CC BY-NC-ND license (http://creativecommons.org/licenses/by-nc-nd/4.0/).

of US$ 25 net per US$ 1 invested in prophylactic chemotherapy [7]. An example of an NTD is African trypanosomiasis (known as sleeping sickness in humans and nagana disease in animals), which is caused by parasites of the genus *Trypanosoma* [8–11]. The infection is transmitted through the bites of tsetse flies (*Glossina* sp.) that have acquired the parasite from infected humans or animals [8–11]. The disease develops in two stages, termed the hemo-lymphatic and neurological stages [8–11]. If left untreated, the disease can lead to behavioral changes, sensory disturbances, coma, and subsequent death [8–11]. Thanks to preventive as well as new therapeutic interventions introduced by the World Health Organization (WHO), the number of sleeping sickness cases has been significantly reduced in recent years [7,8]. However, due to the limited number of drugs available to treat African trypanosomiasis and the emergence of drug-resistant trypanosomes, it is necessary to develop new therapeutics to fight the infection [12].

Another parasitic disease that, although not belonging to the group of NTDs, poses a real threat to global health care is malaria. According to WHO data, in 2021, malaria caused the death of over 600,000 people, making it the deadliest parasitic disease [13]. Malaria is caused by parasites of the genus *Plasmodium*, which are transmitted in their sporozoite form by infected female *Anopheles* mosquitoes [13,14]. Injected sporozoites asymptomatically infect and replicate inside hepatocytes, generating thousands of merozoites that are subsequently released into the bloodstream, where they cyclically infect erythrocytes causing the disease [15]. The initial symptoms of malaria include fever, chills, and headache, but after progression, it can lead to fatigue, confusion, difficulty in breathing, or even death [13,16]. Preventive measures that are currently employed to reduce the spread of the disease include vector control, prophylactic chemotherapies, and the introduction of the RTS,S/AS01 and the R21/Matrix-M malaria vaccines [13,17]. Chloroquine, primaquine and artemisinin-based combination therapy medicines are mainly used to treat the disease, but due to the growing problem of drug resistance, the search for new lead structures for antimalarial drugs is a top priority [13,16,18].

In addition to the licensed uses of **IVR**, the drug has been investigated in experimental therapies against sleeping sickness and malaria, as well as other diseases [3]. **IVR** has been shown to be effective at micromolar concentrations against *T. cruzi* and *T. evansi* [19,20]. The use of **IVR** in mice infected with *T. brucei* was found to be efficacious, resulting in a prolongation of the average survival time of infected animals [21]. This drug was also found to be potent in controlling the spread of tsetse flies, which are the vectors of African trypanosomes [22]. The antimalarial properties of **IVR** have also been extensively studied [23]. **IVR** was able to reduce *P. berghei* infection in human hepatoma cells, with efficacy similar to that of primaquine – the only licensed liver-stage antiplasmodial drug [24,25]. Furthermore, **IVR** exhibited also strong mosquitocidal and larvicidal properties [26]. However, to the best of our knowledge, there are no or only scarce reports in the scientific literature [27,28] on the antitrypanosomal or antiplasmodial activity of **IVR** derivatives, respectively.

Having access to the C13-*epi*-amine precursor of **IVR** (Scheme 1), we now describe the synthesis of a series of amide derivatives modified at position C13 (Scheme 2). We have further extended a library of new compounds with first-in-class analogs with a rearranged oxahydrindene (hexahydrobenzofuran) unit of **IVR** (Schemes 2 and 3). We also report on the trypanocidal and antiplasmodial activities of the **IVR** derivatives using the bloodstream form of *T. brucei brucei* and the hepatic cell-infective form of luciferase-expressing *P. berghei*.

2. Results and discussion

2.1. Analogs design and synthesis

Most of the chemical transformations of avermectin derivatives, including **IVR** (form B1a), described in the scientific literature concern the modification of either the hydroxyl group at position C5 or the sugar moiety, especially the C4″ hydroxyl group (Fig. 1) [29]. It has been shown that C4″-substituted avermectin derivatives exhibited improved bioactivities as well as better pharmacokinetic profiles than the starting compounds [30–34], while the hydroxyl group at position C5 is considered to be crucial for the biological properties [35]. This clearly shows that a rational modification of avermectin derivatives may be a source of promising bioactive compounds. On the other hand, there is less evidence for the effects of chemical modification of other functional groups of **IVR** and other avermectin derivatives, including position C13 (Fig. 1) [27–29,36–39]. Recently, it has been demonstrated that the replacement of the **IVR** sugar moiety with other structural motifs may significantly affect the antimalarial activity of the obtained derivatives [27,28]. Of note, selected sulfonamide-like derivatives of C13-*epi*-aminoivermectin exhibited higher biological activity than **IVR** against *Tetranychus cinnabarinus* and *Aphis craccivora* [38]. On the basis of this information, we designed and synthesized a series of new amide derivatives of **IVR** with an inversed configuration at position C13 to expand the structural diversity at this position and generate attractive candidates for biological investigations.

Starting from **IVR**, a key C13-*epi*-amine precursor was obtained according to protocols published previously [28,36,38,39] with or without minor modifications (Scheme 1). Briefly, **IVR** was treated with a solution of sulfuric acid in methanol to remove the sugar moiety, which resulted in the formation of aglycone **2**, with a 84 % yield (Scheme 1). To mask the C5 functionality, **2** was treated with *tert*-butyldimethylsilyl chloride in the presence of imidazole to give **3** with a 91 % yield (Scheme 1). A complete regioselectivity of this reaction towards the C5 hydroxyl group was observed. Next, the C13 hydroxyl group was oxidized to ketone **4** using Dess-Martin periodinane with a 82 % yield, followed by a reductive amination of the C13 ketone group with ammonium acetate to the amine **5** with a 51 % yield (Scheme 1). The reductive amination was stereoselective and gave only one diastereoisomer, which was confirmed by X-ray analysis (see section 2.2 for details). Gently heating the reaction mixture in the initial phase (imine formation) and extending the reaction time increased its overall yield, compared to that in the original protocol [38]. The spectroscopic data of **2**–**5** were in agreement with those published previously for the same compounds [28,38,39].

Amine **5** was then used in the synthesis of new amides of **IVR** in a reaction with various acyl chlorides in the presence of triethylamine, or using carboxylic acids and HATU as the coupling agent (Scheme 2). After removing the silyl protection group at position C5 with *para*-

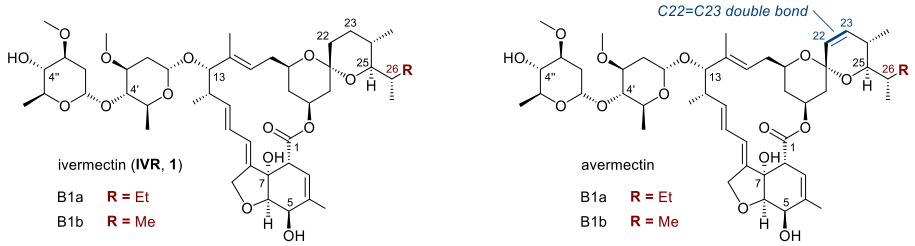

Fig. 1. Chemical structure of ivermectin (left) and avermectin (right).

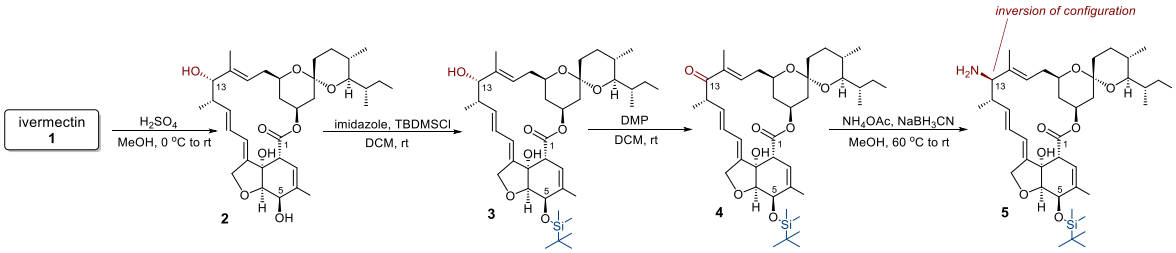

Scheme 1. Synthesis of the C13-*epi*-amine precursor of ivermectin.

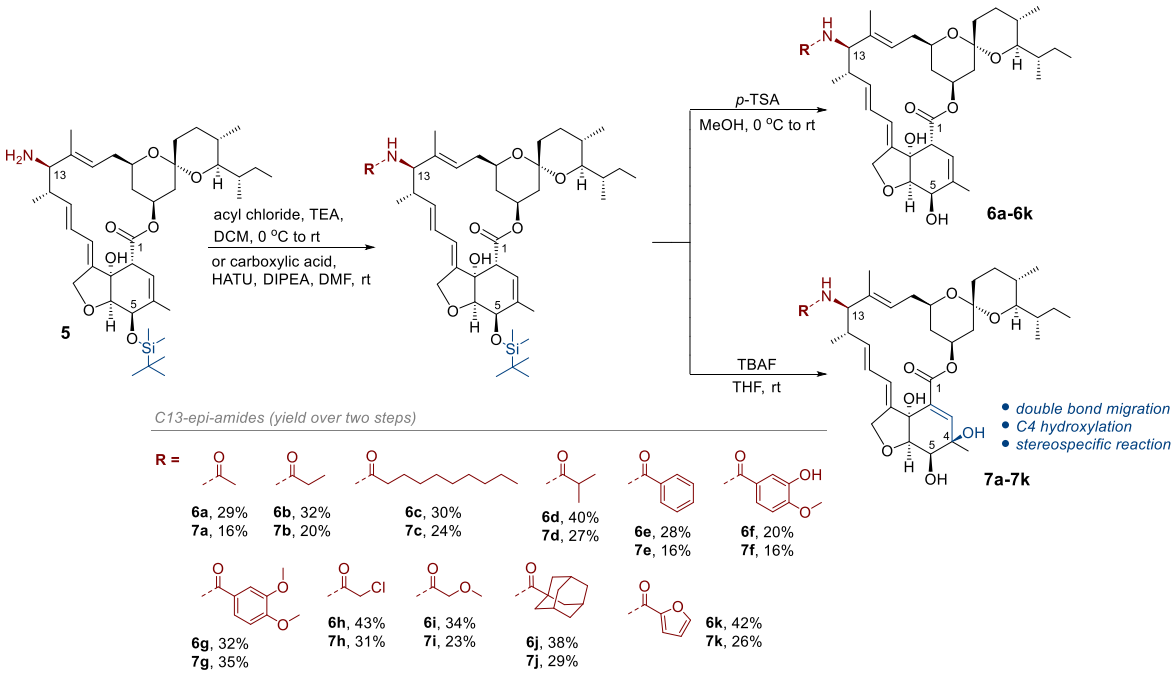

Scheme 2. Synthesis of singly and doubly modified derivatives of ivermectin.

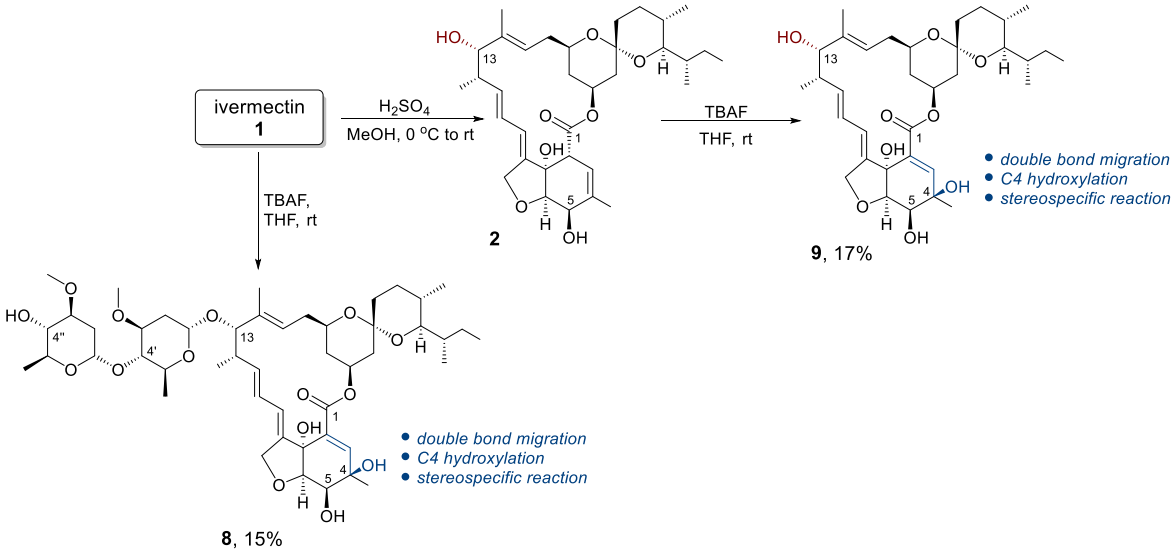

Scheme 3. Synthesis of rearranged ivermectin and its aglycone.

toluenesulfonic acid (*p*-TSA), a series of singly modified **IVR** derivatives **6a**–**6k** was synthesized (Scheme 2). Interestingly, when TBAF was used, instead of *p*-TSA, to deprotect the hydroxyl group from the silyl ether, we observed the formation of the C13-*epi*-amide analogs of rearranged **IVR** (compounds **7a**–**7k**, Scheme 2).

The structure of the unexpectedly rearranged **IVR** was confirmed by the single-crystal X-ray diffraction (scXRD) method. The X-ray structure analysis (see section 2.2 for details) clearly showed that during the reaction the double bond migrated and an additional hydroxyl group was introduced at position C4. Trying to rationally explain this transformation, we have found an interesting study by Buckley et al. [40]. The authors have documented the hydroxylating properties of TBAF, with atmospheric oxygen playing a pivotal role in the reaction and acting as an electrophile [40]. Despite extensive experimentation, including varying the solvent ($CHCl_3$, CH_2Cl_2, MeOH) and reagent (TBAB, TBAI, KF), the rearrangement was exclusively accomplished for TBAF in THF. For **IVR** and its derivatives, apart from TLC analysis, the progress of the reaction can be easily monitored by observing the color of the reaction mixture turning red (Supplementary material, Figure S1). Carrying out the reaction in an "open vessel" or in an inert (argon) atmosphere, we observed a rapid change in the color of the reaction mixture to red only in the "open vessel" variant, which confirmed the key role of atmospheric oxygen in the rearrangement of **IVR**. On the other hand, the addition of hydrogen peroxide resulted in the inhibition of reaction progress (Supplementary material, Figure S1). Based on all these observations, we proposed the mechanism of the rearrangement of **IVR** (Fig. 2). Once the rearrangement reaction conditions were established, the series of derivatives was extended to include the rearranged **IVR** (compound **8**) and its aglycone **9** (Scheme 3).

The purity and structure of the synthesized derivatives of **IVR** were determined using spectroscopic (^{1}H NMR, ^{13}C NMR) and spectrometric (HRMS) methods. In the ^{13}C NMR spectra of **IVR** derivatives, the signals of the highest analytical significance were assigned to the newly introduced carbonyl group of the amide moiety at position C13. Depending on the type of substituent used, the signal from the amide group appeared in the range of 177.6–157.9 ppm, while the signals from the lactone group at the C1 position appeared in a narrow range of 173.4–173.6 ppm or 168.5–169.0 ppm for C13-*epi*-amide derivatives of native or rearranged **IVR**, respectively. The HRMS analysis confirmed the formation of the desired products, with $[M+Na]^+$ as the main peak (intensity 100 %). The NMR spectra of all novel **IVR** derivatives are included in the Supplementary material (Figures S2–S49).

2.2. X-ray diffraction analysis

To elucidate the structure of **IVR** derivatives and establish possible structure-activity relationship (SAR), X-ray diffraction analysis is required. Thus, we characterized derivatives **6a** and **7a** using the scXRD method. This analysis confirmed the (*R*)-stereochemistry at position C13 of the compounds, at which acetamide groups were introduced, and the structure of the rearranged oxahydrindene ring in **7a** (Fig. 3).

In-room conditions, derivative **6a** crystallizes in the monoclinic $P2_1$ space group with two molecules in the asymmetric part of the unit cell ($Z' = 2$, molecules labeled as A and B, Fig. 3). The appearance of two separate **IVR** conformations can be attributed to the labile *sec*-butyl group at position C25, engaged in CH···C intermolecular interactions. The *sec*-butyl group exhibits positional disorder over two equivalent positions, which can be characterized by the torsion angle C28–C27–C26–C25, with values of 112.13° and 66.53° in molecule A and 178.15° and 129.35° in molecule B. The structure of **6a** is porous (the solvent accessible volume calculated with the program Mercury [41] for probe radius 1.2 Å and grid spacing 0.2 Å is equal to 2 % of the total unit-cell volume), which degrades the quality of the single crystals due to the presence of highly disordered, non-stoichiometric amount of solvent (acetone) trapped in the pores.

Interestingly, the rearrangement of the **IVR** molecule does not significantly influence the conformation as observed in **7a** (Fig. 4). The scXRD experiments revealed that the colorless block crystals precipitated from the solution are an acetone solvate of **7a** crystallized in the orthorhombic $P2_12_12$ space group. The co-crystallized acetone molecule is disordered over two positions with a site occupancy factor (SOF) of 0.5.

All **IVR** derivatives share similar structural features – a rigid sixteen-membered lactone ring, a spiroketal comprising two six-membered rings, and a cyclohexene ring fused to a five-membered cyclic ether with two or three hydroxyl groups (Fig. 4) [42,43]. Although the introduction of an additional hydroxyl group at position C4 does not significantly influence the lactone ring and spiroketal conformation, the rearrangement does modify the cyclohexene ring. The hydroxyl group (O4A) at position C4 assumes an axial position, while other substituents maintain their positions – C1 and O5A at position C5 are in equatorial positions while O6A and O7A at positions C6 and C7, respectively, are in axial positions. The migrated double bond in **7a** (from C3–C4 to C2–C3 with distances 1.325(4) Å and 1.493(4) Å, respectively) additionally flattens the cyclohexene with respect to already distorted half-chair conformation observed in **6a** in which C3–C4 and C2–C3 are equal to 1.35(3) Å and 1.50(2) Å in molecule A, and 1.29(3) Å and 1.56(2) Å in molecule B, respectively.

2.3. Biological activity

2.3.1. Trypanocidal activity

The trypanocidal and cytotoxic activities of the newly synthesized **IVR** derivatives were determined with bloodstream forms of *T. b. brucei* and human myeloid HL-60 cells *in vitro*. The antiproliferative activity of the compounds was evaluated with the resazurin cell viability assay as previously described [44].

IVR (compound **1**) itself displayed moderate antitrypanosomal activity with a 50 % growth inhibition (GI_{50}) value in the mid-micromolar range, while aglycone **2** was about twofold more trypanocidal (Table 1). The trypanocidal activity of **IVR** against bloodstream forms of *T. b. brucei* was within the range previously reported for trypomastigote forms of *T. cruzi* ($EC_{50} = 10.4$ (7.0–15.5) μM [20]). The rearranged **IVR** and its aglycone (compounds **8** and **9**) were slightly less trypanocidal than their counterparts (Table 1). All four parent compounds **1**, **2**, **8**, and **9** exhibited similar cytotoxic activity against HL-60 cells with GI_{50} values between 31 and 35 μM (Table 1). Therefore, the selectivity (ratio of cytotoxic to trypanocidal activity) of these four compounds was poor, ranging between 2 and 6 (Table 1).

With the exception of **6h** and **7h**, all other **IVR** derivatives (**6a**–**6g**, **6i**–**6k**, **7a**–**7g**, and **7i**–**7k**) displayed similar antitrypanosomal activity with GI_{50} values ranging between 3.0 and 19.1 μM (Table 1). There was also not much difference in the trypanocidal activity between singly (series **6**) and doubly (series **7**) modified derivatives. Compounds **6h** and

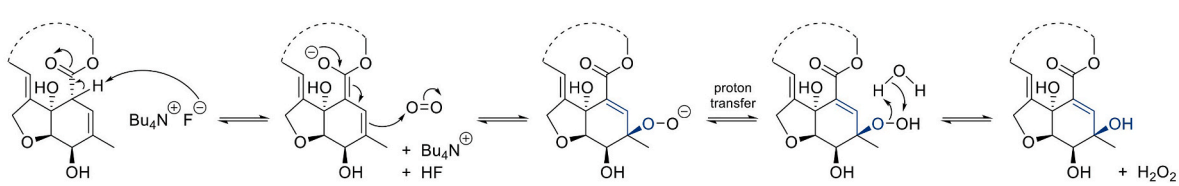

Fig. 2. Proposed mechanism of the rearrangement of the oxahydrindene (hexahydrobenzofuran) ring of ivermectin.

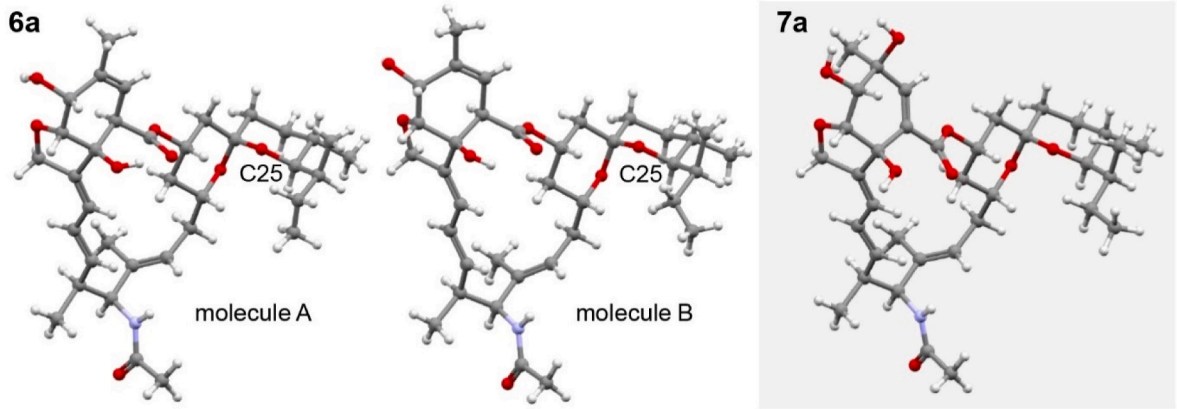

Fig. 3. Ball-and-sticks models of **6a** (molecules A and B) and **7a** from the scXRD experiments. For compound **6a**, only one position of the disordered *sec*-butyl group at position C25 is shown, while in **7a** the co-crystalized acetone is omitted for clarity. Atom color code: C – gray, O – red, N – blue, and H – white.

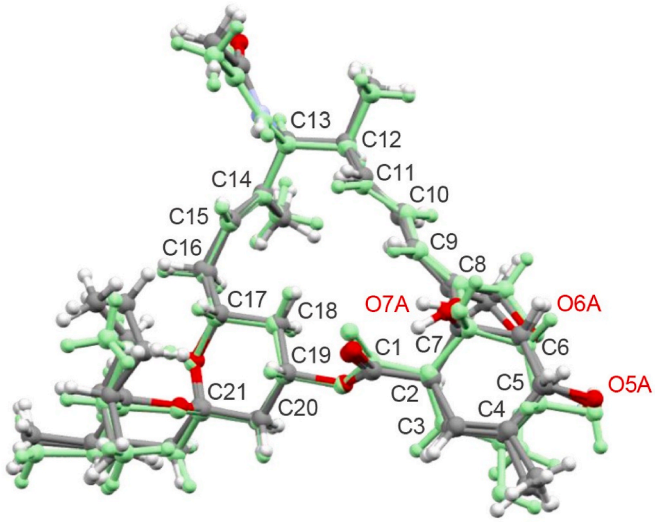

Fig. 4. Molecules A and B of **6a** and molecule **7a** highlighted in green superimposed with respect to the sixteen-membered lactone ring (atom labels are provided).

7h, however, exhibited substantially higher antitrypanosomal activity than any of the other derivatives, with GI_{50} values in the mid-nanomolar range (Table 1). Importantly, the trypanocidal activity of both **6h** and **7h** was within the potency range of suramin and ethidium bromide (commercially known as homidium bromide) (Table 1), two drugs used in the treatment of sleeping sickness and nagana disease, respectively. All the derivatives with weak antitrypanosomal activity exhibited similar cytotoxicity against HL-60 cells with GI_{50} values ranging between 30 and 35 μM (Table 1). By comparison, compounds **6h** and **7h** were about 10 times more cytotoxic (Table 1). It follows that the selectivity indices of all other derivatives were <11 whereas those of **6h** and **7h** were 48 and 67, respectively (Table 1). Therefore, **6h** and **7h** have a similar trypanocidal and selectivity profile as the anti-nagana drug ethidium bromide. Although **6h** and **7h** display similar trypanocidal activity to suramin, the anti-sleeping sickness drug is nonetheless superior as it is non-toxic to human HL-60 cells.

2.3.2. Antiplasmodial activity

To further evaluate the antiparasitic potential of **IVR** derivatives, all four parent compounds **1**, **2**, **8**, and **9**, and two corresponding derivatives **6a** and **7a**, which have been obtained in crystalline form, were screened for antiplasmodial activity against the hepatic infectious stage of *P. berghei in vitro*. To this end, Huh7 cells, a human hepatoma cell line, were infected with luciferase-expressing *P. berghei* parasites in the presence of a range of seven concentrations of the six compounds (Fig. 5). Assessment of the cell confluency revealed that none of the compound concentrations employed was toxic to the host cells, as the cell confluency values obtained were similar to that of the cells exposed to the drug vehicle (DMSO) alone. Infection values were then used to determine the half-maximal inhibitory concentration (IC_{50}) values of each compound (Table 2).

Compound **6a** was less active than the parent compound **1**. The corresponding rearranged **IVR** molecule **8** exhibited also lower activity. On the other hand, this modification resulted in an improved antiplasmodial activity of compounds **9** and **7a**, when compared to that of compounds **2** and **6a**, respectively. Overall, the double modification in **7a** yielded the highest activity against *P. berghei* grown in Huh7 cells, with an IC_{50} value of 0.38 μM for **7a**, which was about 2.5 times lower than that of **IVR** (IC_{50} = 0.91 μM).

2.3.3. Structure-activity relationship considerations

For the newly synthesized **IVR** derivatives, no consistent SAR was observed. While the rearranged parent compounds **8** and **9** displayed lower trypanocidal activity than the native parent compounds **1** and **2**, such a trend was only confirmed for the compound pair **1**/**8** for the plasmodicidal activity (Tables 1 and 2). Moreover, the antitrypanosomal activity of the derivative series **6** and **7** gives also an inconsistent picture – while some series **7** derivatives are less trypanocidal than their series **6** counterparts, other series **7** derivatives display higher trypanocidal activity than their series **6** correspondents (Table 1). Interestingly, doubly modified derivative **7a** was found to be 4 times more plasmodicidal than the corresponding **6a** derivative (Table 2).

From the SAR analysis, it can be concluded that the increased trypanocidal activity of **6h** and **7h** can be attributed to the chlorine atom of the 2-chloroacetamide group. This seems obvious as the structurally related derivatives with an acetamide (compounds **6a** and **7a**), a propionamide (compounds **6b** and **7b**), and an isobutyramide (compounds **6d** and **7d**) group were about 100 times less trypanocidal than **6h** and **7h** (Table 1). The increased trypanocidal activity of **6h** and **7h** may be due to the greater electronegativity (EN) of the $–CH_2Cl$ group (EN = 2.47 [45]) compared to that of the $–CH_3$, $–CH_2CH_3$, and $–CH(CH_3)_2$ groups, which all have similar EN values (EN = 2.27, 2.28, and 2.28, respectively [45]). Therefore, it would be interesting to see whether a more electronegative group (e.g., $–CF_3$; EN = 3.46 [45]) can further increase the trypanocidal activity of C13-*epi*-amide derivatives of **IVR**.

3. Conclusions

Synthesis of a series of novel C13-*epi*-amide derivatives of native or

Table 1
GI_{50} values and ratios of ivermectin derivatives for *T. b. brucei* and HL-60 cells.

No.	R or compound	*T. b. brucei*	HL-60	Selectivity	No.	*T. b. brucei*	HL-60	Selectivity
		GI_{50} (μM)[a]	GI_{50} (μM)[a]	GI_{50} ratio[b]		GI_{50} (μM)[a]	GI_{50} (μM)[a]	GI_{50} ratio[b]
Native oxahydrindene ring					**Rearranged oxahydrindene ring**			
1	ivermectin	14.6 ± 6.4	31.3 ± 1.8	2.1	**8**	20.0 ± 3.8	32.0 ± 0.7	1.6
2	aglycone	6.1 ± 3.5	35.2 ± 1.9	5.8	**9**	12.1 ± 1.9	31.5 ± 1.7	2.6
C13-*epi*-amides of native ivermectin					**C13-*epi*-amides of rearranged ivermectin**			
	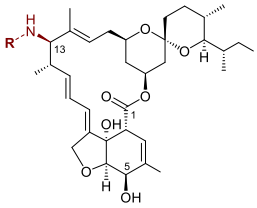					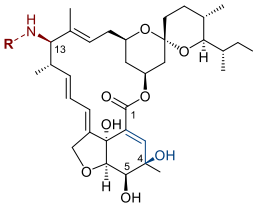		
6a		5.5 ± 2.4	32.0 ± 1.9	5.8	**7a**	7.5 ± 1.1	33.8 ± 1.0	4.5
6b		7.4 ± 5.1	32.1 ± 0.5	4.3	**7b**	8.1 ± 3.6	35.2 ± 2.0	4.3
6c		9.3 ± 5.2	30.0 ± 1.7	3.2	**7c**	4.1 ± 0.6	32.7 ± 1.8	7.8
6d		10.2 ± 7.7	33.8 ± 1.7	3.3	**7d**	6.6 ± 1.9	33.5 ± 1.3	5.1
6e		8.6 ± 5.0	30.8 ± 1.6	3.6	**7e**	4.3 ± 0.6	30.2 ± 1.2	7.0
6f	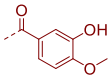	3.9 ± 0.8	32.0 ± 3.0	8.2	**7f**	4.1 ± 0.7	32.6 ± 2.8	8.0
6g	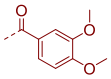	5.8 ± 3.3	32.2 ± 2.7	5.6	**7g**	5.0 ± 1.1	32.1 ± 1.5	6.4
6h		0.063 ± 0.039	3.0 ± 0.2	47.6	**7h**	0.064 ± 0.033	4.3 ± 1.6	67.2
6i		14.4 ± 6.3	33.5 ± 0.7	2.3	**7i**	18.2 ± 0.4	32.1 ± 1.0	1.8
6j		19.1 ± 7.6	31.2 ± 2.2	1.6	**7j**	3.0 ± 0.1	30.8 ± 0.4	10.3
6k		10.2 ± 5.1	31.6 ± 1.6	3.1	**7k**	4.7 ± 0.4	32.8 ± 0.8	7.0
suramin[c]		0.036 ± 0.015	>100	>2778				
ethidium bromide[c]		0.086 ± 0.014	5.8 ± 0.7	67.4				

[a] Data shown are mean values ± SD of three independent experiments.
[b] GI_{50} ratio = GI_{50}(HL-60)/GI_{50}(*T. b. brucei*).
[c] Reference controls.

rearranged ivermectin (**IVR**) is described. The practical as well as scalable synthetic approach provides convenient access to material suitable for further development of this class of compounds that are interesting from both medicinal chemistry and cell biology points of view. Of the newly synthesized derivatives, two compounds (**6h** and **7h**) displayed promising antiparasitic activity against *T. b. brucei*. In particular, the antitrypanosomal activity of **6h** and **7h** is intriguing as their trypanocidal activity and selectivity profile is similar to that of the anti-nagana drug ethidium bromide. It would be beneficial if the potential carcinogenic ethidium bromide could be replaced by the C13-*epi*-2-chloroacetamides of either native (compound **6h**) or rearranged **IVR** (compound **7h**) for the treatment of animal trypanosomiasis. However, before the compounds can be used as anti-nagana drugs, they would need to be tested in animal models for their *in vivo* efficacy. Given the close relationship between *Leishmania* spp. and *Trypanosoma* spp., it would be interesting to test the **IVR** derivatives also on those parasites.

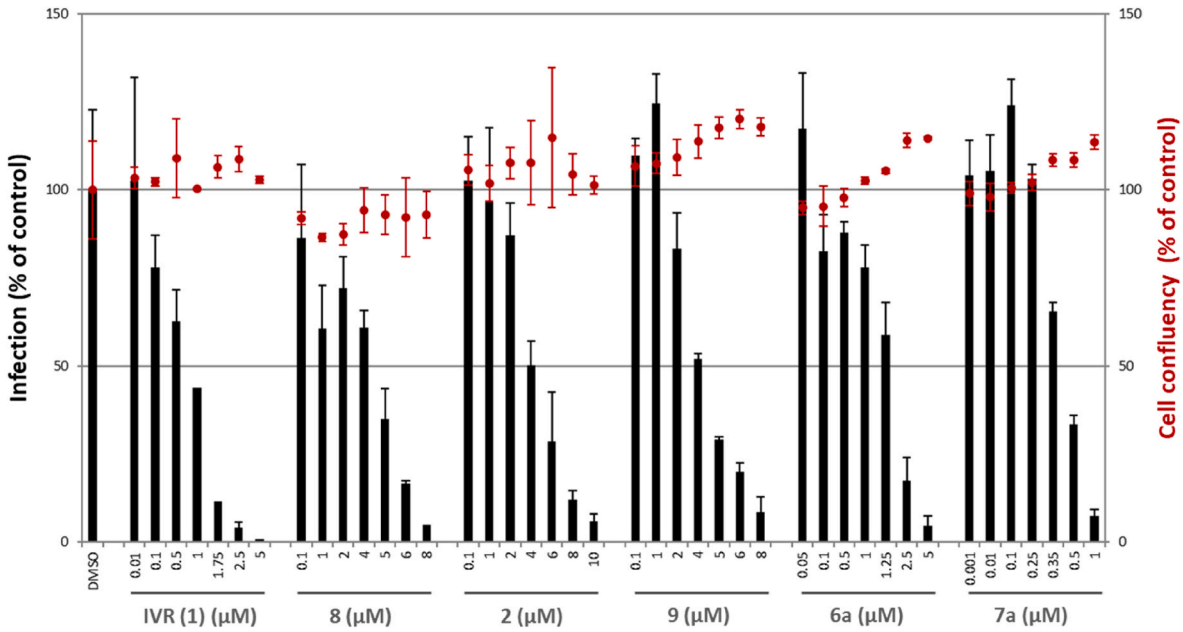

Fig. 5. Dose-dependent response of ivermectin **1**, its aglycone **2**, and derivatives **6a**, **7a**, **8**, and **9**, against the hepatic stage of *P. berghei*. Total parasite load (infection scale, bars) and cell viability (cell confluency scale, dots) are shown. Calculated IC_{50} values are presented in Table 2.

Table 2
IC_{50} values of selected compounds against the hepatic stage of *P. berghei*.

Native oxahydrindene ring		Rearranged oxahydrindene ring	
No.	IC_{50} (μM)[a]	No.	IC_{50} (μM)[a]
ivermectin **1**	0.911 ± 0.029	**8**	4.721 ± 0.266
aglycone **2**	5.452 ± 1.637	**9**	2.852 ± 1.008
6a	1.523 ± 0.576	**7a**	**0.379 ± 0.002**

[a] Data shown are mean values ± SD of two or three independent experiments.

On the other hand, compound **7a** showed better *in vitro* antiplasmodial activity against *P. bergei* than **IVR**. The findings of this study suggest that doubly modified **IVR** derivatives may be suitable lead compounds for the rational development of new and effective antiparasitic drug candidates.

4. Experimental

4.1. General procedures

Ivermectin (**IVR**, form B1a) was purchased from Trimen Chemicals S. A. All reagents, except Dess-Martin periodinane (DMP), which was freshly prepared according to the protocol published by Frigerio et al. [46], were commercially available and purchased from two sources – Merck or Trimen Chemicals S.A., as well as used without further purification. Compounds **2**–**5** were resynthesized according to protocols published previously by other authors [28,38,39]. A detailed description of the general procedures, measurement parameters, and equipment can be found in the Supplementary material.

4.2. Synthesis of ivermectin aglycone (compound 2)

IVR (4.95 g, 5.66 mmol, 1.0 equiv.) was dissolved in methanol (79.2 mL) and the solution was cooled in an ice bath. Then, concentrated sulfuric acid (0.8 mL) was added dropwise to the reaction mixture. The solution changed its color to greenish and after a few hours to yellow. After 20 h, the reaction mixture was concentrated on a rotary evaporator, diluted with CH_2Cl_2, and extracted with an aqueous solution of sodium carbonate (0.1 M). The collected organic layers were subsequently concentrated *in vacuo*. Purification on silica gel using the CombiFlash system (0 %→30 % EtOAc/$CHCl_3$) gave the pure aglycone **2** as a clear oil. After twice evaporation to dryness with *n*-pentane, the oily product was completely converted into a white amorphous solid (2.79 g, 84 % yield). The spectroscopic data were in agreement with previously published data [28,39].

4.3. Protection of the C5 hydroxyl group of ivermectin aglycone (compound 3)

To a stirred solution of **2** (2.00 g, 3.41 mmol, 1.0 equiv.) in anhydrous CH_2Cl_2 (40 mL), imidazole (2.32 g, 34.07 mmol, 10.0 equiv.) was added. After the imidazole had dissolved, *tert*-butyldimethylsilyl chloride (1.13 g, 7.50 mmol, 2.2 equiv.) was added in one portion. The reaction mixture was stirred at room temperature for 24 h. After this time, the reaction mixture was concentrated on a rotary evaporator to dryness. Purification on silica gel using the CombiFlash system (0 %→10 % EtOAc/$CHCl_3$) gave the pure product **3** as a clear oil. After twice evaporation to dryness with *n*-pentane, the oily product was completely converted into a yellow amorphous solid (2.17 g, 91 % yield). The spectroscopic data were in agreement with previously published data [28,39].

4.4. Synthesis of C13 ketone of C5-protected ivermectin aglycone (compound 4)

To a stirred solution of **3** (4.90 g, 6.99 mmol, 1.0 equiv.) in anhydrous CH_2Cl_2 (60 mL), *tert*-butyl alcohol (517 mg, 6.99 mmol, 1.0 equiv.) was added. Next, Dess-Martin periodinane (freshly prepared) (4.45 g, 10.49 mmol, 1.5 equiv.) was added to the reaction mixture and stirring was continued for 24 h. The reaction mixture was then diluted with CH_2Cl_2 and extracted with an aqueous solution of sodium thiosulfate (0.5 M). The collected organic layers were subsequently concentrated *in vacuo*. Purification on silica gel using the CombiFlash system (0 %→5 % EtOAc/$CHCl_3$) gave the pure ketone **4** as a clear oil. After twice evaporation to dryness with *n*-pentane, the oily product was completely converted into a white amorphous solid (3.43 g, 82 % yield). The spectroscopic data were in agreement with previously published data [39].

4.5. Synthesis of the C13-epi-amine of C5-protected ivermectin aglycone (compound 5)

According to Ref. [38], to a stirred solution of **4** (3.43 g, 4.91 mmol, 1.0 equiv.) in methanol (40 mL), ammonium acetate (3.78 g, 49.1 mmol, 10.0 equiv.) was added. The reaction mixture was then heated at 60 °C for an hour. After this time, sodium cyanoborohydride (618 mg, 9.82 mmol, 2.0 equiv.) dissolved in methanol (5 mL) was added dropwise to the reaction mixture. After 24 h, the reaction mixture was concentrated on a rotary evaporator, diluted with CH_2Cl_2, and extracted with an aqueous solution of sodium carbonate (0.1 M). The collected organic layers were subsequently concentrated *in vacuo*. Purification on silica gel using the CombiFlash system (0 %→100 % EtOAc/$CHCl_3$) gave the pure product **5** as a clear oil. After twice evaporation to dryness with *n*-pentane, the oily product was completely converted into a yellow amorphous solid (1.75 g, 51 % yield).

4.6. General procedure for preparation of C13-epi-amide derivatives of native ivermectin (analogs 6a–6e and 6h–6k)

Precursor **5** (250 mg, 0.36 mmol, 1.0 equiv.) was dissolved in CH_2Cl_2 (5 mL) and triethylamine (108 mg, 1.07 mmol, 3.0 equiv.) was added. Next, the respective acyl chloride (0.43 mmol, 1.2 equiv.) was added to the reaction mixture, and stirring was continued at room temperature for 24 h. After this time, the reaction mixture was diluted with CH_2Cl_2 and extracted with an aqueous solution of sulfuric acid (pH = 1) and then with water. The collected organic layers were subsequently concentrated *in vacuo*. Purification on silica gel using the CombiFlash system (0 %→100 % EtOAc/$CHCl_3$) gave the C13-*epi*-amide products as clear oils.

To remove the C5-protecting group, the appropriate C13-*epi*-amide product was dissolved in methanol (10 mL) and *para*-toluenesulfonic acid hydrate (80 mg, 0.46 mmol, 1.3 equiv.) was added. After 2 h, the organic solvent was evaporated, diluted with CH_2Cl_2, and extracted with an aqueous solution of sodium carbonate (0.1 M). Next, the collected organic layers were subsequently concentrated *in vacuo*. Purification on silica gel using the CombiFlash system (0 %→100 % EtOAc/$CHCl_3$) gave the pure products **6a–6e** and **6h–6k** as clear oils. After twice evaporation to dryness with *n*-pentane, the oily products were completely converted into white amorphous solids.

*C13-epi-acetamide of ivermectin **6a**:* 65 mg, 29 % yield (over two steps). Isolated as a white amorphous solid, a single spot by TLC. UV-active and strains green with PMA; ^{1}H NMR (400 MHz, $CDCl_3$) δ 5.83–5.72 (m, 2H), 5.68 (d, J = 9.6 Hz, 1H), 5.42–5.32 (m, 2H), 5.22 (tt, J = 11.2, 4.8 Hz, 1H), 4.91 (dd, J = 10.5, 4.7 Hz, 1H), 4.61 (qd, J = 14.5, 1.4 Hz, 2H), 4.41 (d, J = 8.8 Hz, 1H), 4.25–4.20 (m, 1H), 3.89 (d, J = 6.2 Hz, 1H), 3.57–3.47 (m, 1H), 3.20 (dd, J = 4.6, 2.2 Hz, 1H), 3.11 (dd, J = 9.0, 1.3 Hz, 1H), 2.71 (dtd, J = 17.2, 6.7, 3.7 Hz, 1H), 2.28–2.13 (m, 2H), 2.05 (s, 2H), 1.90 (ddd, J = 12.2, 4.9, 1.5 Hz, 1H), 1.82–1.78 (m, 2H), 1.64–0.65 (m, 30H) ppm; ^{13}C NMR (101 MHz, $CDCl_3$) δ 173.5, 169.8, 141.1, 137.8, 136.6, 135.6, 125.9, 119.6, 117.8, 117.4, 97.4, 80.2, 78.9, 77.1, 68.4, 68.2, 67.6, 67.0, 58.1, 45.5, 41.1, 38.1, 36.6, 35.7, 35.4, 34.4, 31.2, 27.9, 27.3, 23.3, 19.9, 19.0, 17.4, 15.6, 12.5, 11.8 ppm; HRMS (ESI$^+$) *m/z*: [M+Na]$^+$ Calcd for $C_{36}H_{53}NNaO_8^+$ 650.3669; Found 650.3686.

*C13-epi-propionamide of ivermectin **6b**:* 73 mg, 32 % yield (over two steps). Isolated as a white amorphous solid, a single spot by TLC. UV-active and strains green with PMA; ^{1}H NMR (401 MHz, $CDCl_3$) δ 5.88–5.77 (m, 2H), 5.61 (d, J = 9.8 Hz, 1H), 5.47–5.36 (m, 2H), 5.27 (ddd, J = 16.4, 11.7, 4.9 Hz, 1H), 4.93 (dd, J = 10.0, 5.4 Hz, 1H), 4.66 (q, J = 14.4 Hz, 2H), 4.47 (d, J = 9.4 Hz, 1H), 4.27 (d, J = 6.0 Hz, 1H), 3.94 (d, J = 6.2 Hz, 1H), 3.56 (td, J = 9.9, 5.2 Hz, 1H), 3.25 (dd, J = 4.4, 2.1 Hz, 1H), 3.16 (d, J = 7.8 Hz, 1H), 2.81–2.71 (m, 1H), 2.37–2.15 (m, 5H), 2.03–0.66 (m, 34H) ppm; ^{13}C NMR (101 MHz, $CDCl_3$) δ 173.5, 173.4, 141.1, 137.9, 136.8, 135.7, 125.8, 119.7, 117.8, 117.3, 97.4, 80.2, 79.0, 76.9, 68.5, 68.2, 67.6, 67.0, 57.6, 45.6, 41.2, 38.2, 36.6, 35.7, 35.4, 34.4, 31.2, 29.9, 27.9, 27.3, 19.9, 18.9, 17.4, 15.6, 12.4, 11.9, 10.1 ppm; HRMS (ESI$^+$) *m/z*: [M+Na]$^+$ Calcd for $C_{37}H_{55}NNaO_8^+$ 664.3820; Found 664.3855.

*C13-epi-decanamide of ivermectin **6c**:* 79 mg, 30 % yield (over two steps). Isolated as a white amorphous solid, a single spot by TLC. UV-active and strains green with PMA; ^{1}H NMR (400 MHz, $CDCl_3$) δ 5.83–5.66 (m, 2H), 5.49 (d, J = 9.8 Hz, 1H), 5.41–5.29 (m, 2H), 5.29–5.17 (m, 1H), 4.88 (dd, J = 9.4, 6.0 Hz, 1H), 4.68–4.54 (m, 2H), 4.43 (d, J = 9.5 Hz, 1H), 4.22 (dd, J = 6.4, 0.9 Hz, 1H), 3.89 (d, J = 6.2 Hz, 1H), 3.55–3.46 (m, 1H), 3.20 (dt, J = 4.4, 1.6 Hz, 1H), 3.14–3.09 (m, 1H), 2.71 (tt, J = 10.5, 6.7 Hz, 1H), 2.29–2.10 (m, 4H), 1.99–0.59 (m, 49H) ppm; ^{13}C NMR (101 MHz, $CDCl_3$) δ 173.5, 172.8, 141.1, 137.9, 136.9, 135.7, 125.9, 119.6, 117.8, 117.2, 97.4, 80.2, 78.9, 68.4, 68.2, 67.6, 67.0, 57.7, 45.6, 41.2, 38.1, 37.1, 36.6, 35.7, 35.4, 34.4, 31.8, 31.2, 29.4, 29.34, 29.31, 29.2, 27.9, 27.3, 26.1, 22.6, 19.9, 19.0, 17.3, 15.6, 14.0, 12.5, 11.8 ppm, one signal overlapped; HRMS (ESI$^+$) *m/z*: [M+Na]$^+$ Calcd for $C_{44}H_{69}NNaO_8^+$ 762.4915; Found 762.4936.

*C13-epi-isobutyramide of ivermectin **6d**:* 94 mg, 40 % yield (over two steps). Isolated as a white amorphous solid, a single spot by TLC. UV-active and strains green with PMA; ^{1}H NMR (400 MHz, $CDCl_3$) δ 5.84–5.70 (m, 2H), 5.51 (d, J = 9.7 Hz, 1H), 5.42–5.30 (m, 1H), 5.30–5.09 (m, 2H), 4.87 (dd, J = 9.0, 6.4 Hz, 2H), 4.61 (q, J = 14.4 Hz, 1H), 4.42 (d, J = 9.1 Hz, 2H), 4.22 (d, J = 5.5 Hz, 1H), 3.89 (d, J = 6.2 Hz, 1H), 3.76–3.63 (m, 1H), 3.55–3.46 (m, 1H), 3.21 (dd, J = 4.5, 2.2 Hz, 1H), 3.12 (dd, J = 9.3, 1.4 Hz, 1H), 2.72 (dddd, J = 13.7, 10.5, 6.7, 3.4 Hz, 1H), 2.44 (tt, J = 11.2, 5.5 Hz, 1H), 2.27–2.11 (m, 2H), 1.91 (dd, J = 11.7, 4.5 Hz, 1H), 1.85–0.54 (m, 35H) ppm; ^{13}C NMR (101 MHz, $CDCl_3$) δ 176.4, 173.5, 141.1, 137.9, 136.9, 135.6, 125.9, 119.6, 117.8, 117.1, 97.4, 80.3, 78.9, 76.7, 68.5, 68.2, 67.6, 67.0, 57.3, 45.5, 41.1, 38.2, 36.6, 36.0, 35.7, 35.4, 34.3, 31.2, 27.9, 27.3, 19.9, 19.8, 19.7, 18.9, 17.4, 15.6, 12.4, 11.9 ppm; HRMS (ESI$^+$) *m/z*: [M+Na]$^+$ Calcd for $C_{38}H_{57}NNaO_8^+$ 678.3976; Found 678.3996.

*C13-epi-benzamide of ivermectin **6e**:* 69 mg, 28 % yield (over two steps). Isolated as a white amorphous solid, a single spot by TLC. UV-active and strains green with PMA; ^{1}H NMR (400 MHz, $CDCl_3$) δ 7.79–7.66 (m, 2H), 7.52–7.33 (m, 3H), 6.11 (d, J = 9.7 Hz, 1H), 5.89–5.69 (m, 2H), 5.47–5.39 (m, 1H), 5.37–5.30 (m, 1H), 5.30–5.11 (m, 2H), 5.01–4.94 (m, 1H), 4.70–4.56 (m, 3H), 4.27–4.20 (m, 1H), 3.88 (dd, J = 13.8, 5.6 Hz, 1H), 3.77–3.64 (m, 1H), 3.56–3.45 (m, 1H), 3.22 (td, J = 4.4, 2.1 Hz, 1H), 3.08 (dd, J = 9.2, 1.1 Hz, 1H), 2.82 (dtd, J = 17.2, 6.8, 3.9 Hz, 1H), 2.22 (t, J = 8.4 Hz, 2H), 1.98–0.40 (m, 30H) ppm; ^{13}C NMR (101 MHz, $CDCl_3$) δ 173.6, 167.1, 141.3, 137.9, 136.8, 135.4, 134.5, 131.7, 128.7 (2C), 126.8 (2C), 126.1, 119.6, 117.8, 117.5, 97.4, 80.3, 78.9, 68.5, 68.3, 67.6, 67.0, 58.3, 45.6, 41.2, 38.5, 36.6, 35.7, 35.4, 34.4, 31.2, 29.7, 27.9, 27.3, 19.9, 19.1, 17.4, 15.7, 12.4, 11.9 ppm; HRMS (ESI$^+$) *m/z*: [M+Na]$^+$ Calcd for $C_{41}H_{55}NNaO_8^+$ 712.3820; Found 712.3844.

*C13-epi-2-chloroacetamide of ivermectin **6h**:* 102 mg, 43 % yield (over two steps). Isolated as a white amorphous solid, a single spot by TLC. UV-active and strains green with PMA; ^{1}H NMR (401 MHz, $CDCl_3$) δ 6.72 (d, J = 10.0 Hz, 1H), 5.90–5.70 (m, 3H), 5.47–5.30 (m, 4H), 4.99–4.92 (m, 1H), 4.67 (qd, J = 14.5, 1.9 Hz, 3H), 4.47 (dd, J = 9.7, 2.1 Hz, 1H), 4.30–4.26 (m, 2H), 4.15 (d, J = 4.2 Hz, 2H), 4.12–4.02 (m, 2H), 3.97–3.93 (m, 2H), 3.75–3.70 (m, 1H), 3.62–3.52 (m, 1H), 3.29–3.24 (m, 2H), 3.20–3.08 (m, 2H), 2.85–2.76 (m, 1H), 2.46–0.46 (m, 24H) ppm; ^{13}C NMR (101 MHz, $CDCl_3$) δ 173.5, 165.3, 141.5, 137.9, 136.1, 134.8, 126.3, 119.5, 117.9, 117.8, 97.5, 80.3, 79.0, 76.9, 68.5, 68.3, 67.6, 67.0, 58.2, 45.6, 42.9, 41.2, 38.4, 36.6, 35.7, 35.4, 34.3, 31.2, 28.0, 27.3, 19.9, 18.9, 17.4, 15.5, 12.4, 11.9 ppm; HRMS (ESI$^+$) *m/z*: [M+Na]$^+$ Calcd for $C_{36}H_{52}ClNNaO_8^+$ 684.3274, 686.3245; Found 684.3282, 686.3319.

*C13-epi-2-methoxyacetamide of ivermectin **6i**:* 80 mg, 34 % yield (over two steps). Isolated as a white amorphous solid, a single spot by TLC. UV-active and strains green with PMA; ^{1}H NMR (400 MHz, $CDCl_3$) δ 6.63 (d, J = 10.2 Hz, 1H), 5.83–5.74 (m, 2H), 5.39–5.30 (m, 2H), 5.24 (td, J = 11.3, 5.6 Hz, 1H), 4.88 (dd, J = 9.2, 6.2 Hz, 1H), 4.61 (q, J = 13.8 Hz,

2H), 4.44 (d, $J = 9.8$ Hz, 1H), 4.22 (dd, $J = 5.9$, 0.7 Hz, 1H), 3.96–3.85 (m, 3H), 3.52 (dd, $J = 12.3$, 6.7 Hz, 1H), 3.45 (s, 3H), 3.21 (dd, $J = 4.5$, 2.2 Hz, 1H), 3.12 (dd, $J = 8.9$, 1.2 Hz, 1H), 2.72 (dtd, $J = 17.3$, 6.8, 3.9 Hz, 1H), 2.29–2.16 (m, 2H), 2.04–0.53 (m, 32H) ppm; ^{13}C NMR (101 MHz, $CDCl_3$) δ 173.5, 169.1, 141.0, 137.8, 136.4, 135.4, 125.9, 119.6, 117.8, 117.5, 97.4, 80.3, 78.9, 76.8, 71.8, 68.5, 68.2, 67.6, 67.0, 59.1, 57.0, 45.5, 41.1, 38.4, 36.5, 35.6, 35.3, 34.3, 31.1, 27.9, 27.3, 19.9, 18.9, 17.3, 15.6, 12.3, 11.9 ppm; HRMS (ESI$^+$) *m/z*: [M+Na]$^+$ Calcd for $C_{37}H_{55}NNaO_9^+$ 680.3769; Found 680.3794.

*C13-epi-adamantane-1-carboxamide of ivermectin **6j**:* 102 mg, 38 % yield (over two steps). Isolated as a white amorphous solid, a single spot by TLC. UV-active and strains green with PMA; ^{1}H NMR (401 MHz, $CDCl_3$) δ 5.83–5.73 (m, 2H), 5.61 (d, $J = 9.7$ Hz, 1H), 5.37–5.34 (m, 1H), 5.28 (ddt, $J = 16.3$, 11.2, 4.1 Hz, 2H), 4.86–4.80 (m, 1H), 4.62 (qd, $J = 14.4$, 1.2 Hz, 2H), 4.41 (d, $J = 8.8$ Hz, 1H), 4.25–4.20 (m, 1H), 3.90 (d, $J = 6.2$ Hz, 1H), 3.53–3.44 (m, 1H), 3.24–3.20 (m, 1H), 3.13 (dd, $J = 9.0$, 1.3 Hz, 1H), 2.76–2.67 (m, 1H), 2.20 (t, $J = 8.7$ Hz, 2H), 2.05–1.97 (m, 4H), 1.96–0.58 (m, 43H) ppm; ^{13}C NMR (101 MHz, $CDCl_3$) δ 177.2, 173.6, 141.1, 138.0, 137.1, 135.7, 125.9, 119.7, 117.9, 117.1, 97.5, 80.4, 79.0, 76.5, 68.6, 68.3, 67.6, 67.1, 56.9, 45.6, 41.2, 41.1, 39.6 (3C), 38.4, 36.6, 36.5 (3C), 35.7, 35.4, 34.3, 31.2, 28.1 (3C), 28.0, 27.3, 19.9, 19.0, 17.4, 15.6, 12.3, 12.2 ppm; HRMS (ESI$^+$) *m/z*: [M+Na]$^+$ Calcd for $C_{45}H_{65}NNaO_8^+$ 770.4602; Found 770.4635.

*C13-epi-furan-2-carboxamide of ivermectin **6k**:* 102 mg, 42 % yield (over two steps). Isolated as a white amorphous solid, a single spot by TLC. UV-active and strains green with PMA; ^{1}H NMR (401 MHz, $CDCl_3$) δ 7.46 (dd, $J = 1.8$, 0.8 Hz, 1H), 7.08 (dd, $J = 3.5$, 0.8 Hz, 1H), 6.48 (dd, $J = 3.5$, 1.8 Hz, 1H), 6.39 (d, $J = 10.1$ Hz, 1H), 5.85–5.72 (m, 2H), 5.45 (ddd, $J = 14.0$, 10.4, 5.8 Hz, 1H), 5.35 (s, 1H), 5.30–5.20 (m, 1H), 4.98 (t, $J = 7.8$ Hz, 1H), 4.69–4.55 (m, 3H), 4.25–4.20 (m, 1H), 3.90 (d, $J = 6.2$ Hz, 1H), 3.55–3.47 (m, 1H), 3.22 (dp, $J = 4.7$, 2.4 Hz, 1H), 3.11–3.05 (m, 1H), 2.83–2.74 (m, 1H), 2.24–2.16 (m, 2H), 2.03–0.52 (m, 32H) ppm; ^{13}C NMR (101 MHz, $CDCl_3$) δ 173.5, 157.9, 147.7, 143.8, 141.2, 137.8, 136.5, 135.4, 126.0, 119.6, 117.8, 117.7, 114.5, 112.3, 97.4, 80.3, 79.0, 76.9, 68.5, 68.2, 67.6, 67.0, 57.4, 45.6, 41.1, 38.5, 36.6, 35.6, 35.3, 34.3, 31.1, 27.9, 27.3, 19.8, 19.0, 17.3, 15.6, 12.3, 11.8 ppm; HRMS (ESI$^+$) *m/z*: [M+Na]$^+$ Calcd for $C_{39}H_{53}NNaO_9^+$ 702.3613; Found 702.3641.

4.7. General procedure for preparation of C13-epi-amide derivatives of native ivermectin (analogs 6f–6g)

To a stirred solution of the respective carboxylic acid (0.36 mmol, 1.0 equiv.) in DMF (10 mL), *N*,*N*-diisopropylethylamine (279 mg, 2.16 mmol, 6.0 equiv.) and 2-(7-aza-1*H*-benzotriazol-1-yl)-1,1,3,3-tetramethylurea hexafluorophosphate (HATU) (176 mg, 0.46 mmol, 1.3 equiv.) were added and the reaction mixture was stirred at room temperature for 15 min. Next, precursor **5** (250 mg, 0.36 mmol, 1.0 equiv.) was added and the stirring was continued for 24 h. After this time, the reaction mixture was diluted with CH_2Cl_2 and extracted with an aqueous solution of sulfuric acid (pH = 1) and then with water. The collected organic layers were subsequently concentrated *in vacuo*. Purification on silica gel using the CombiFlash system (0 %→100 % EtOAc/$CHCl_3$) gave the C13-*epi*-amide products as clear oils.

To remove the C5-protecting group, the corresponding C13-*epi*-amide product was dissolved in methanol (10 mL) and *para*-toluenesulfonic acid hydrate (80 mg, 0.46 mmol, 1.3 equiv.) was added. After 2 h, the organic solvent was evaporated, diluted with CH_2Cl_2 and extracted with an aqueous solution of sodium carbonate (0.1 M). Next, the collected organic layers were subsequently concentrated *in vacuo*. Purification on silica gel using the CombiFlash system (0 %→100 % EtOAc/$CHCl_3$) gave the pure products **6f–6g** as clear oils. After twice evaporation to dryness with *n*-pentane, the oily products were completely converted into white amorphous solids.

*C13-epi-3-hydroxy-4-methoxybenzamide of ivermectin **6f**:* 53 mg, 20 % yield (over two steps). Isolated as a white amorphous solid, a single spot by TLC. UV-active and strains green with PMA; ^{1}H NMR (400 MHz, $CDCl_3$) δ 7.76–7.64 (m, 1H), 7.32 (tt, $J = 5.5$, 2.7 Hz, 1H), 6.85 (ddd, $J = 11.6$, 10.1, 6.3 Hz, 1H), 6.09–5.99 (m, 1H), 5.86–5.71 (m, 2H), 5.49–5.39 (m, 1H), 5.35 (dd, $J = 3.5$, 2.2 Hz, 1H), 5.30–5.23 (m, 1H), 4.99–4.92 (m, 1H), 4.71–4.55 (m, 2H), 4.28–4.19 (m, 1H), 4.18–4.06 (m, 1H), 3.95–3.77 (m, 4H), 3.51 (ddd, $J = 12.6$, 8.3, 6.8 Hz, 1H), 3.21 (dt, $J = 5.2$, 2.6 Hz, 1H), 3.08 (d, $J = 8.9$ Hz, 1H), 2.85–2.76 (m, 1H), 2.38–2.28 (m, 1H), 2.25–2.11 (m, 2H), 2.01–0.61 (m, 32H) ppm; ^{13}C NMR (101 MHz, $CDCl_3$) δ 173.6, 166.6, 149.4, 145.6, 141.2, 137.9, 136.9, 135.6, 126.1, 119.7, 117.9, 117.5, 116.3, 113.0, 112.0, 110.2, 110.0, 97.4, 80.3, 78.9, 68.5, 68.3, 67.7, 67.1, 58.2, 56.1, 45.6, 41.2, 38.5, 36.6, 35.7, 35.4, 34.4, 31.2, 27.9, 27.3, 19.9, 19.1, 17.4, 15.7, 12.4, 11.8 ppm; HRMS (ESI$^+$) *m/z*: [M+Na]$^+$ Calcd for $C_{42}H_{57}NNaO_{10}^+$ 758.3875; Found 758.3890.

*C13-epi-3,4-dimethoxybenzamide of ivermectin **6g**:* 86 mg, 32 % yield (over two steps). Isolated as a white amorphous solid, a single spot by TLC. UV-active and strains green with PMA; ^{1}H NMR (400 MHz, $CDCl_3$) δ 7.46 (d, $J = 2.0$ Hz, 1H), 7.32 (dd, $J = 8.3$, 2.1 Hz, 1H), 6.89 (dd, $J = 8.4$, 2.5 Hz, 1H), 6.13 (d, $J = 9.8$ Hz, 1H), 5.93–5.77 (m, 2H), 5.53–5.44 (m, 1H), 5.42–5.38 (m, 1H), 5.34–5.25 (m, 1H), 5.04–4.98 (m, 1H), 4.74–4.61 (m, 3H), 4.29–4.25 (m, 1H), 3.97–3.87 (m, 9H), 3.59–3.50 (m, 1H), 3.29–3.25 (m, 1H), 3.12 (dd, $J = 9.1$, 1.6 Hz, 1H), 2.91–2.80 (m, 1H), 2.31–2.20 (m, 2H), 2.05–0.56 (m, 30H) ppm; ^{13}C NMR (101 MHz, $CDCl_3$) δ 173.5, 166.6, 151.9, 149.2, 141.3, 137.9, 136.9, 135.5, 127.1, 126.1, 119.6, 118.6, 117.8, 117.4, 111.0, 110.2, 97.4, 80.3, 79.0, 76.9, 68.5, 68.2, 67.6, 67.0, 58.3, 56.02, 55.99, 45.6, 41.2, 38.5, 36.6, 35.7, 35.4, 34.3, 31.1, 27.9, 27.3, 19.9, 19.1, 17.3, 15.6, 12.4, 11.8 ppm; HRMS (ESI$^+$) *m/z*: [M+Na]$^+$ Calcd for $C_{43}H_{59}NNaO_{10}^+$ 772.4031; Found 772.4055.

4.8. General procedure for preparation of C13-epi-amide derivatives of rearranged ivermectin (analogs 7a–7k)

The corresponding C13-*epi*-amide of **IVR** with protected C5 hydroxyl group (1.0 equiv.) (please see section 4.6 and 4.7 for synthetic details) was dissolved in anhydrous THF. Next, tetra-*n*-butylammonium fluoride (TBAF) (3.0 equiv.) was added in one portion and the reaction mixture was stirred at room temperature for 3 days. After this time, the solvent was evaporated under reduced pressure. Purification on silica gel using the CombiFlash system (0 %→100 % EtOAc/$CHCl_3$) gave the pure products **7a–7k** as clear oils. After twice evaporation to dryness with *n*-pentane, the oily products were completely converted into white amorphous solids.

*C13-epi-acetamide of rearranged ivermectin **7a**:* 37 mg, 16 % yield (over two steps). Isolated as a white amorphous solid, a single spot by TLC. UV-active and strains green with PMA; ^{1}H NMR (400 MHz, $CDCl_3$) δ 6.19 (s, 1H), 6.11 (dt, $J = 4.5$, 1.9 Hz, 1H), 5.80 (dd, $J = 14.5$, 11.2 Hz, 1H), 5.65 (d, $J = 9.9$ Hz, 1H), 5.46 (dd, $J = 14.5$, 10.6 Hz, 1H), 5.29–5.22 (m, 1H), 4.92 (ddd, $J = 11.3$, 2.3, 1.2 Hz, 1H), 4.77 (s, 1H), 4.52 (ddd, $J = 22.5$, 14.3, 2.2 Hz, 2H), 4.45 (s, 1H), 4.10 (dd, $J = 7.7$, 2.5 Hz, 2H), 3.61 (tdd, $J = 11.2$, 4.3, 2.1 Hz, 1H), 3.18 (dd, $J = 9.1$, 1.5 Hz, 1H), 2.74 (dtd, $J = 17.1$, 6.7, 3.7 Hz, 1H), 2.43–0.58 (m, 37H) ppm; ^{13}C NMR (101 MHz, $CDCl_3$) δ 169.9, 168.6, 139.8, 139.1, 136.3, 129.4, 126.6, 122.7, 117.4, 97.4, 82.6, 78.1, 77.2, 73.5, 71.7, 69.2, 68.0, 66.9, 58.1, 40.4, 38.0, 36.5, 35.8, 35.4, 34.7, 31.2, 29.7, 27.9, 27.4, 23.4, 22.8, 18.9, 17.4, 15.5, 12.6, 11.8 ppm; HRMS (ESI$^+$) *m/z*: [M+Na]$^+$ Calcd for $C_{36}H_{53}NNaO_9^+$ 666.3613; Found 666.3634.

*C13-epi-propionamide of rearranged ivermectin **7b**:* 47 mg, 20 % yield (over two steps). Isolated as a white amorphous solid, a single spot by TLC. UV-active and strains green with PMA; ^{1}H NMR (401 MHz, $CDCl_3$) δ 6.17 (s, 1H), 6.10 (dt, $J = 11.0$, 2.3 Hz, 1H), 5.79 (dd, $J = 14.5$, 11.2 Hz, 1H), 5.68 (d, $J = 9.9$ Hz, 1H), 5.45 (dd, $J = 14.5$, 10.6 Hz, 1H), 5.30–5.20 (m, 1H), 4.92–4.85 (m, 1H), 4.77 (s, 1H), 4.57–4.41 (m, 3H), 4.09 (s, 2H), 3.63–3.54 (m, 1H), 3.20–3.06 (m, 2H), 2.78–2.68 (m, 1H), 2.48–0.58 (m, 38H) ppm; ^{13}C NMR (101 MHz, $CDCl_3$) δ 173.7, 168.6, 139.9, 139.3, 136.4, 136.3, 129.3, 126.5, 122.6, 117.3, 97.3, 82.7, 78.0,

73.4, 71.6, 69.1, 67.9, 66.9, 57.8, 40.4, 38.1, 36.5, 35.8, 35.4, 34.6, 31.2, 29.9, 29.6, 27.9, 27.3, 22.8, 18.8, 17.4, 15.4, 12.4, 11.9, 10.2 ppm; HRMS (ESI$^+$) *m/z*: [M+Na]$^+$ Calcd for $C_{37}H_{55}NNaO_9^+$ 680.3769; Found 680.3785.

*C13-epi-decanamide of rearranged ivermectin **7c**:* 65 mg, 24 % yield (over two steps). Isolated as a white amorphous solid, a single spot by TLC. UV-active and strains green with PMA; ^{1}H NMR (401 MHz, $CDCl_3$) δ 6.19 (s, 1H), 6.12 (dt, J = 3.1, 2.2 Hz, 1H), 5.81 (dd, J = 14.6, 11.2 Hz, 1H), 5.54 (d, J = 9.5 Hz, 1H), 5.44 (dd, J = 14.6, 10.5 Hz, 1H), 5.33–5.22 (m, 1H), 4.90 (dd, J = 10.0, 3.4 Hz, 1H), 4.75 (s, 1H), 4.53 (ddd, J = 14.1, 12.9, 2.7 Hz, 3H), 4.48–4.44 (m, 1H), 4.11 (s, 1H), 3.60 (td, J = 10.4, 4.1 Hz, 1H), 3.20–3.12 (m, 1H), 2.79–2.70 (m, 1H), 2.40–0.48 (m, 53H) ppm; ^{13}C NMR (101 MHz, $CDCl_3$) δ 173.2, 169.0, 140.3, 139.4, 136.9, 136.6, 129.8, 126.9, 123.0, 117.6, 97.7, 82.9, 78.4, 77.5, 73.9, 72.0, 69.5, 68.3, 67.3, 58.1, 40.8, 38.4, 37.5, 36.8, 36.1, 35.8, 35.0, 32.1, 31.6, 29.8, 29.72, 29.67, 29.6, 28.3, 27.7, 26.4, 23.2, 23.0, 19.2, 17.7, 15.8, 14.4, 12.9, 12.1 ppm; HRMS (ESI$^+$) *m/z*: [M+Na]$^+$ Calcd for $C_{44}H_{69}NNaO_9^+$ 778.4865; Found 778.4876.

*C13-epi-isobutyramide of rearranged ivermectin **7d**:* 65 mg, 27 % yield (over two steps). Isolated as a white amorphous solid, a single spot by TLC. UV-active and strains green with PMA; ^{1}H NMR (400 MHz, $CDCl_3$) δ 6.11 (s, J = 9.9 Hz, 1H), 6.03 (dt, J = 11.0, 2.3 Hz, 1H), 5.72 (dd, J = 14.5, 11.2 Hz, 1H), 5.56 (d, J = 9.8 Hz, 1H), 5.37 (dd, J = 14.6, 10.6 Hz, 1H), 5.20 (ddd, J = 16.3, 11.2, 4.9 Hz, 1H), 4.85–4.76 (m, 1H), 4.68 (s, 1H), 4.44 (ddd, J = 23.0, 14.5, 2.4 Hz, 2H), 4.37 (d, J = 9.8 Hz, 1H), 4.08–3.97 (m, 2H), 3.52 (ddd, J = 10.8, 4.7, 2.2 Hz, 1H), 3.10 (d, J = 7.9 Hz, 1H), 2.66 (tt, J = 10.5, 6.7 Hz, 1H), 2.43 (tt, J = 13.7, 6.8 Hz, 1H), 2.34–0.35 (m, 40H) ppm; ^{13}C NMR (101 MHz, $CDCl_3$) δ 176.8, 168.6, 139.9, 139.2, 136.5, 136.2, 129.3, 126.6, 122.6, 117.2, 97.4, 82.6, 78.0, 76.8, 73.4, 71.6, 69.1, 67.9, 66.9, 57.4, 40.3, 38.2, 36.5, 36.0, 35.7, 35.4, 34.6, 31.2, 27.9, 27.3, 22.8, 19.9, 19.7, 18.8, 17.4, 15.4, 12.4, 11.9 ppm; HRMS (ESI$^+$) *m/z*: [M+Na]$^+$ Calcd for $C_{38}H_{57}NNaO_9^+$ 694.3926; Found 694.3918.

*C13-epi-benzamide of rearranged ivermectin **7e**:* 40 mg, 16 % yield (over two steps). Isolated as a white amorphous solid, a single spot by TLC. UV-active and strains green with PMA; ^{1}H NMR (400 MHz, $CDCl_3$) δ 7.85–7.70 (m, 2H), 7.53–7.35 (m, 3H), 6.19–6.07 (m, 2H), 5.85–5.74 (m, 1H), 5.48 (dd, J = 14.6, 10.6 Hz, 1H), 5.29–5.19 (m, 1H), 4.96–4.89 (m, 1H), 4.70 (s, 1H), 4.66–4.59 (m, 1H), 4.49 (qd, J = 14.3, 2.3 Hz, 2H), 4.09–4.00 (m, 1H), 3.57–3.47 (m, 1H), 3.08 (dd, J = 9.3, 1.4 Hz, 1H), 2.84–2.75 (m, 1H), 2.27–2.15 (m, 2H), 2.00–0.38 (m, 34H) ppm; ^{13}C NMR (101 MHz, $CDCl_3$) δ 168.7, 167.3, 140.2, 139.0, 136.5, 136.0, 134.5, 131.7, 129.5, 128.7 (2C), 126.9 (2C), 126.8, 122.6, 117.5, 97.4, 82.6, 78.1, 73.6, 71.7, 69.2, 68.0, 66.9, 58.3, 40.4, 38.5, 36.6, 35.7, 35.4, 34.7, 31.2, 29.7, 27.9, 27.3, 22.9, 19.0, 17.4, 15.6, 12.4, 11.8 ppm; HRMS (ESI$^+$) *m/z*: [M+Na]$^+$ Calcd for $C_{41}H_{55}NNaO_9^+$ 728.3769; Found 728.3738.

*C13-epi-3-hydroxy-4-methoxybenzamide of rearranged ivermectin **7f**:* 43 mg, 16 % yield (over two steps). Isolated as a white amorphous solid, a single spot by TLC. UV-active and strains green with PMA; ^{1}H NMR (400 MHz, $CDCl_3$) δ 7.74–7.61 (m, 1H), 7.35–7.26 (m, 1H), 6.87–6.76 (m, 1H), 6.13–6.00 (m, 2H), 5.76 (dd, J = 14.4, 11.2 Hz, 1H), 5.51–5.40 (m, 1H), 5.26–5.16 (m, 1H), 4.94–4.85 (m, 1H), 4.63–4.53 (m, 1H), 4.45 (ddd, J = 16.5, 14.5, 2.3 Hz, 2H), 4.08–4.00 (m, 2H), 3.92–3.72 (m, 4H), 3.55–3.45 (m, 1H), 3.10–3.02 (m, 1H), 2.95–2.84 (m, 1H), 2.80–2.70 (m, 1H), 2.27–2.08 (m, 2H), 1.99–0.47 (m, 33H) ppm; ^{13}C NMR (101 MHz, $CDCl_3$) δ 168.6, 166.9, 149.5, 145.7, 140.1, 139.1, 136.5, 136.0, 129.4, 127.5, 126.8, 122.6, 119.5, 117.4, 113.2, 110.3, 97.3, 82.6, 78.1, 73.5, 71.7, 69.1, 68.0, 66.9, 58.3, 56.1, 40.4, 38.5, 36.5, 35.8, 35.4, 34.7, 31.2, 29.6, 27.9, 27.3, 22.8, 19.0, 17.4, 15.5, 12.4, 11.8 ppm; HRMS (ESI$^+$) *m/z*: [M+Na]$^+$ Calcd for $C_{42}H_{57}NNaO_{11}^+$ 774.3824; Found 774.3834.

*C13-epi-3,4-dimethoxybenzamide of rearranged ivermectin **7g**:* 96 mg, 35 % yield (over two steps). Isolated as a white amorphous solid, a single spot by TLC. UV-active and strains green with PMA; ^{1}H NMR (400 MHz, CDCl3) δ 7.39 (d, J = 2.0 Hz, 1H), 7.29 (dd, J = 8.3, 2.0 Hz, 1H), 6.88–6.83 (m, 1H), 6.10–6.02 (m, 2H), 5.77 (dd, J = 14.5, 11.2 Hz, 1H), 5.45 (dd, J = 14.4, 10.6 Hz, 1H), 5.21 (ddd, J = 16.1, 11.1, 4.8 Hz, 2H), 4.89 (dd, J = 10.2, 4.7 Hz, 1H), 4.59 (d, J = 9.4 Hz, 1H), 4.52–4.38 (m, 3H), 4.07–3.99 (m, 2H), 3.92–3.80 (m, 8H), 3.49 (dd, J = 9.8, 5.1 Hz, 1H), 3.12–3.01 (m, 1H), 2.81–2.71 (m, 1H), 2.26–2.13 (m, 2H), 2.00–0.53 (m, 30H) ppm; ^{13}C NMR (101 MHz, CDCl3) δ 168.7, 166.9, 151.9, 149.2, 140.1, 139.2, 136.6, 136.0, 129.3, 127.0, 126.8, 122.5, 118.8, 117.4, 110.9, 110.2, 97.3, 82.6, 78.1, 73.4, 71.6, 69.2, 67.9, 66.9, 58.4, 56.0 (2C), 40.4, 38.5, 36.5, 35.7, 35.4, 34.6, 31.2, 29.6, 27.9, 27.3, 22.8, 19.0, 17.3, 15.5, 12.4, 11.8 ppm; HRMS (ESI$^+$) *m/z*: [M+Na]$^+$ Calcd for $C_{43}H_{59}NNaO_{11}^+$ 788.3980; Found 788.4003.

*C13-epi-2-chloroacetamide of rearranged ivermectin **7h**:* 75 mg, 31 % yield (over two steps). Isolated as a white amorphous solid, a single spot by TLC. UV-active and strains green with PMA; ^{1}H NMR (401 MHz, $CDCl_3$) δ 6.80–6.69 (m, 1H), 6.24–6.12 (m, 2H), 5.83 (dd, J = 14.5, 11.2 Hz, 1H), 5.44 (dd, J = 14.8, 10.6 Hz, 1H), 5.38–5.31 (m, 2H), 4.98–4.89 (m, 1H), 4.55 (qd, J = 14.5, 2.9 Hz, 2H), 4.49–4.44 (m, 1H), 4.17–4.05 (m, 6H), 3.79–3.71 (m, 1H), 3.68–3.58 (m, 1H), 3.23–3.10 (m, 2H), 2.82–2.75 (m, 1H), 2.45–0.61 (m, 30H) ppm; ^{13}C NMR (101 MHz, $CDCl_3$) δ 168.7, 165.5, 140.4, 138.7, 135.8, 135.4, 129.6, 127.0, 122.5, 117.7, 97.4, 82.6, 73.7, 71.7, 69.2, 68.0, 66.9, 58.3, 53.4, 42.9, 40.4, 38.4, 36.6, 35.8, 35.5, 34.7, 31.2, 29.7, 28.0, 27.4, 22.9, 18.8, 17.4, 15.5, 12.5, 11.9 ppm; HRMS (ESI$^+$) *m/z*: [M+Na]$^+$ Calcd for $C_{36}H_{52}ClNNaO_9^+$ 700.3223, 702.3194; Found 700.3244, 702.3289.

*C13-epi-2-methoxyacetamide of rearranged ivermectin **7i**:* 55 mg, 23 % yield (over two steps). Isolated as a white amorphous solid, a single spot by TLC. UV-active and strains green with PMA; ^{1}H NMR (401 MHz, $CDCl_3$) δ 6.70 (d, J = 10.3 Hz, 1H), 6.20–6.11 (m, 2H), 5.80 (dd, J = 14.4, 11.3 Hz, 1H), 5.44 (dd, J = 14.3, 10.7 Hz, 1H), 5.37–5.26 (m, 1H), 4.89 (dd, J = 10.5, 3.5 Hz, 1H), 4.76 (s, 1H), 4.60–4.46 (m, 3H), 4.10 (dd, J = 14.2, 2.4 Hz, 2H), 4.03–3.92 (m, 2H), 3.66–3.57 (m, 1H), 3.53 (s, 3H), 3.18 (d, J = 8.1 Hz, 1H), 2.75 (ddd, J = 10.4, 6.9, 3.8 Hz, 1H), 2.33–2.19 (m, 2H), 2.07–0.57 (m, 32H) ppm; ^{13}C NMR (101 MHz, $CDCl_3$) δ 169.3, 168.7, 140.0, 139.0, 136.2, 136.0, 129.5, 126.6, 122.6, 117.5, 97.4, 82.7, 78.1, 77.0, 73.5, 71.9, 71.6, 69.2, 68.0, 66.9, 59.2, 57.1, 40.4, 38.4, 36.5, 35.8, 35.4, 34.7, 31.2, 28.0, 27.4, 22.8, 18.9, 17.4, 15.5, 12.4, 11.9 ppm; HRMS (ESI$^+$) *m/z*: [M+Na]$^+$ Calcd for $C_{37}H_{55}NNaO_{10}^+$ 696.3718; Found 696.3740.

*C13-epi-adamantane-1-carboxamide of rearranged ivermectin **7j**:* 79 mg, 29 % yield (over two steps). Isolated as a white amorphous solid, a single spot by TLC. UV-active and strains green with PMA; ^{1}H NMR (400 MHz, $CDCl_3$) δ 6.13 (s, 1H), 6.10–6.05 (m, 1H), 5.75 (dd, J = 14.5, 11.2 Hz, 1H), 5.65 (d, J = 9.7 Hz, 1H), 5.34 (dd, J = 14.5, 10.7 Hz, 1H), 5.30–5.22 (m, 1H), 4.77 (dd, J = 9.9, 4.6 Hz, 1H), 4.70 (s, 1H), 4.53–4.41 (m, 2H), 4.39 (d, J = 9.2 Hz, 1H), 4.09–3.99 (m, 1H), 3.52 (td, J = 9.8, 4.9 Hz, 1H), 3.14 (dd, J = 9.0, 1.3 Hz, 1H), 2.72–2.65 (m, 1H), 2.33–0.47 (m, 50H) ppm; ^{13}C NMR (101 MHz, $CDCl_3$) δ 177.6, 168.7, 140.1, 139.1, 136.8, 136.0, 129.3, 126.7, 122.4, 117.0, 97.4, 82.6, 78.1, 76.5, 71.6, 69.1, 68.0, 66.9, 57.0, 41.1, 40.3, 39.5 (3C), 38.3, 36.5, 36.4 (3C), 35.7, 35.3, 34.6, 31.2, 28.1 (3C), 28.03, 27.96, 27.2, 22.8, 18.8, 17.4, 15.4, 12.3, 12.1 ppm; HRMS (ESI$^+$) *m/z*: [M+Na]$^+$ Calcd for $C_{45}H_{65}NNaO_9^+$ 786.4552; Found 786.4571.

*C13-epi-furan-2-carboxamide of rearranged ivermectin **7k**:* 65 mg, 26 % yield (over two steps). Isolated as a white amorphous solid, a single spot by TLC. UV-active and strains green with PMA; ^{1}H NMR (400 MHz, $CDCl_3$) δ 7.53–7.48 (m, 1H), 7.44–7.35 (m, 1H), 7.11–7.03 (m, 1H), 6.49 (dd, J = 3.5, 1.8 Hz, 1H), 6.46–6.39 (m, 1H), 6.16–6.05 (m, 2H), 5.79 (dd, J = 14.5, 11.2 Hz, 1H), 5.47 (dd, J = 14.5, 10.6 Hz, 1H), 5.30–5.20 (m, 1H), 4.93 (dd, J = 9.7, 5.2 Hz, 1H), 4.72 (s, 1H), 4.56 (d, J = 10.3 Hz, 1H), 4.48 (ddd, J = 22.2, 14.2, 2.3 Hz, 2H), 4.05 (dd, J = 9.2, 2.5 Hz, 2H), 3.59–3.50 (m, 1H), 3.12–3.05 (m, 1H), 2.80–2.72 (m, 1H), 2.38–0.49 (m, 33H) ppm; ^{13}C NMR (101 MHz, $CDCl_3$) δ 168.7, 158.1, 147.6, 144.0, 140.0, 139.1, 136.2, 136.0, 129.4, 126.7, 122.6, 117.7, 114.7, 112.3, 97.4, 82.6, 78.1, 77.1, 73.5, 71.6, 69.2, 68.0, 66.9, 57.5, 40.4, 38.5, 36.5, 35.7, 35.4, 34.6, 31.2, 27.9, 27.4, 22.8, 18.9, 17.4, 15.5, 12.4, 11.8 ppm; HRMS (ESI$^+$) *m/z*: [M+Na]$^+$ Calcd for

$C_{39}H_{53}NNaO_{10}^{+}$ 718.3562; Found 718.3581.

4.9. General procedure for preparation of rearranged ivermectin and its aglycone (analogs 8–9)

To a stirred solution of **IVR** or its aglycone **2** (1.0 equiv.) in anhydrous THF, tetra-*n*-butylammonium fluoride (TBAF) (3.0 equiv.) was added and the reaction mixture was stirred at room temperature for 3 days. After this time, the organic solvent was evaporated under reduced pressure. Purification on silica gel using the CombiFlash system (0 %→ 100 % EtOAc/$CHCl_3$) gave the pure products **8**–**9** as clear oils. After twice evaporation to dryness with *n*-pentane, the oily products were completely converted into white amorphous solids.

*Rearranged ivermectin **8**:* 76 mg, 15 % yield. Isolated as a white amorphous solid, a single spot by TLC. UV-active and strains green with PMA; ^{1}H NMR (401 MHz, $CDCl_3$) δ 6.13 (q, J = 7.9 Hz, 2H), 5.85–5.58 (m, 2H), 5.41–5.26 (m, 2H), 4.90 (d, J = 10.0 Hz, 1H), 4.76 (d, J = 29.7 Hz, 2H), 4.49 (q, 2H), 4.06 (s, 2H), 3.89 (s, 1H), 3.84–3.58 (m, 5H), 3.51–3.31 (m, 11H), 3.17 (dt, J = 31.5, 9.0 Hz, 5H), 2.49–2.39 (m, 1H), 2.26 (dd, J = 38.3, 11.9 Hz, 5H), 1.96–0.50 (m, 33H) ppm; ^{13}C NMR (101 MHz, $CDCl_3$) δ 168.9, 138.7, 138.5, 138.4, 134.7, 129.5, 125.4, 123.1, 118.0, 98.4, 97.4, 94.7, 82.8, 81.8, 80.3, 79.3, 78.2, 78.0, 76.6, 75.9, 73.2, 71.6, 69.2, 68.1, 67.10, 67.05, 56.5, 56.31, 56.25, 40.3, 39.6, 36.7, 35.7, 35.4, 34.4, 34.3, 34.1, 31.2, 28.0, 27.2, 22.6, 20.1, 18.3, 17.6, 17.4, 15.1, 12.4, 12.0 ppm; HRMS (ESI$^+$) *m/z*: [M+Na]$^+$ Calcd for $C_{48}H_{74}NaO_{15}^{+}$ 913.4920; Found 913.4926.

*Rearranged ivermectin aglycone **9**:* 70 mg, 17 % yield. Isolated as a white amorphous solid, a single spot by TLC. UV-active and strains green with PMA; ^{1}H NMR (401 MHz, $CDCl_3$) δ 6.16–6.07 (m, 2H), 5.78–5.63 (m, 2H), 5.32–5.22 (m, 2H), 4.93 (s, 1H), 4.57–4.44 (m, 2H), 4.07 (s, 2H), 3.96 (s, 1H), 3.69 (td, J = 11.6, 4.8 Hz, 1H), 3.17 (d, J = 8.0 Hz, 1H), 2.48 (p, J = 7.4 Hz, 1H), 2.34–2.18 (m, 2H), 2.05–0.54 (m, 33H) ppm; ^{13}C NMR (101 MHz, $CDCl_3$) δ 168.5, 138.5, 138.2, 137.5, 129.5, 125.5, 123.3, 117.1, 97.3, 82.8, 77.8, 77.0, 73.3, 71.6, 69.0, 68.1, 67.1, 40.4, 39.9, 36.6, 35.8, 35.5, 34.5, 31.2, 28.0, 27.4, 22.6, 19.1, 17.4, 14.5, 12.5, 11.7 ppm; two signals overlapped, HRMS (ESI$^+$) *m/z*: [M+Na]$^+$ Calcd for $C_{34}H_{50}NaO_9^{+}$ 625.3347; Found 625.3366.

4.10. X-ray measurements

For X-ray diffraction, suitable crystals of **6a** and **7a** were grown by slow evaporation of a saturated solution of the **IVR** derivatives in acetone at room temperature. Single-crystal X-ray diffraction (scXRD) data were collected using a four-circle Oxford-Diffraction SuperNova and Xcalibur both equipped with an EOS-CCD detector. The X-ray radiation source applied for the investigation of **6a** single-crystals was CuKα (λ = 1.54184 Å) while for **7a** single-crystals AgKα (λ = 0.56087 Å) radiation was used.

The collected data were processed and corrected for absorption with CrysAlisPro 171.42.59. The structures were solved by direct methods and refined by full-matrix least-squares on F^2 using the SHELXS and SHELXL with OLEX2 software package [47–49]. Anisotropic displacement factors were generally applied for non-hydrogen atoms. Hydrogen atoms in **6a** were placed at calculated positions and refined using a riding model, while in **7a** most of their positions (despite solvate molecule and terminal methyl groups: C2B, C12a, C24A, and C28) were derived from difference Fourier maps. The U_{iso} values of the hydrogen atoms were constrained to 1.2 times the U_{eq} for carbon atoms and 1.5 for other carrier atoms. The MASK procedure was implemented in **6a** using OLEX2 program to remove the residual electron density located inside void volumes, resulting from the presence of disordered solvent molecules (presumably water molecules). Structural drawings were prepared using the program Mercury CSD 4.0 [50]. Atom numbers were adapted from Ref. [43].

The description of hydrogen bonds can be found in the Supplementary material. The H-bond patterns in molecules **6a** and **7a** are also shown in the Supplementary material (Figure S50). The final crystal data are in Table S1 (Supplementary material) and have been deposited in the Cambridge Structural Database as supplementary publications CCDS 2294517 (compound **6a**) and 2294516 (compound **7a**). Copies of this information can be obtained free of charge from The Director, CCDC, 12 Union Road, Cambridge, CB2 1EZ, UK; E-mail: deposit@ccdc.cam.ac.uk or http://www.ccdc.cam.ac.uk.

4.11. In vitro biological studies

4.11.1. Trypanocidal and cytotoxic assays

Trypanosoma brucei brucei bloodstream form 221a [51] and human promyelocytic leukemia HL-60 cells [52] were employed for the determination of the trypanocidal and cytotoxic activity of test compounds. Cells were seeded at densities of 1×10^{-4} mL^{-1} (*T. b. brucei*) and 5×10^{-4} mL^{-1} (HL-60) in the presence of various concentrations of test compounds (tenfold dilutions from 100 μM to 1 nM) and 0.9 % DMSO in 200 μL of Baltz medium [53] supplemented with 16.7 % bovine serum in 96-well plates. Controls were incubated in the bovine serum-supplemented medium containing only 0.9 % DMSO. The cultures were incubated at 37 °C in a humidified atmosphere containing 5 % CO_2. After 24 h, 20 μL of a 0.5 mM resazurin solution in PBS was added and the incubation was continued for another 48 h. Then, the absorbance of the cultures was read on a BioTek ELx808 microplate reader using a test wavelength of 570 nm and a reference wavelength of 630 nm. The 50 % growth inhibition (GI_{50}) values (the concentration of a compound required to reduce the growth rate of cells by 50 % compared to the control) were calculated by linear interpolation according to the method described by Huber and Koella [54].

4.11.2. Hepatic stage antiplasmodial activity

The antiplasmodial activity of test compounds was assessed *in vitro* with *P. berghei*-infected human hepatoma cells (Huh7 cells), as previously described [27,28]. Briefly, Huh7 cells were cultured in Roswell Park Memorial Institute (RPMI)-1640 medium supplemented with 10 % (v/v) fetal calf serum (FCS), 1 % v/v penicillin/streptomycin, 1 % v/v glutamine, 1 % v/v non-essential amino acids and 10 mM HEPES, pH 7, and incubated at 37 °C and 5 % CO_2. Cells were seeded at 1×10^4 cells per well in a 96-well plate and incubated until the following day. Compound stock solutions were prepared at 10 mM in DMSO and serially diluted in medium (supplemented with 50 μg mL^{-1} gentamicin and 0.8 μg mL^{-1} amphotericin B) to achieve the desired test concentrations. As a control, DMSO was diluted in the same medium to mimic the highest percentage of the drug vehicle employed in the assay. One hour prior to infection, the culture medium was replaced by the compound solutions, and the cells were incubated as described above. Luciferase-expressing *P. berghei* sporozoites (PbGFP-Luccon [55]), obtained from salivary glands dissected from infected female *Anopheles stephensi* mosquitoes, were added to the cells at a 1:1 ratio, and the plates were centrifuged at 1800×*g* for 5 min at room temperature. At 46 h post-infection (hpi), the cell confluency was assessed by the AlamarBlue assay (Invitrogen, UK), according to the manufacturer's instructions. Finally, at 48 hpi, the parasite load was assessed in a bioluminescence assay (Firefly Luciferase Assay kit 2.0, Biotium, USA), according to the manufacturer's instructions. Nonlinear regression analysis was employed to fit the normalized results of the dose-response curves, and the half-maximal inhibitory concentration (IC_{50}) values were determined using GraphPad Prism 8.0 (GraphPad software, La Jolla California USA).

Declaration of competing interest

The authors declare that they have no known competing financial interests or personal relationships that could have appeared to influence the work reported in this paper.

Data availability

Data will be made available on request.

Acknowledgments

The synthesis of ivermectin derivatives was financially supported by a Diamond Grant (0159/DIA/2020/49) funded by the Polish Ministry of Education and Science (MEiN) to M.S. D.F. wishes to acknowledge FCT – Fundação para a Ciência e Tecnologia, I.P., for the financial support (project reference 2022.02624.PTDC).

Appendix A. Supplementary data

Supplementary data to this article can be found online at https://doi.org/10.1016/j.ejmech.2023.115951.

References

[1] A. Crump, Ivermectin: enigmatic multifaceted 'wonder' drug continues to surprise and exceed expectations, J. Antibiot. 70 (2017) 495–505.
[2] W.C. Campbell, History of avermectin and ivermectin, with notes on the history of other macrocyclic lactone antiparasitic agents, Curr. Pharmaceut. Biotechnol. 13 (2012) 853–865.
[3] M. Sulik, M. Antoszczak, A. Huczyński, D. Steverding, Antiparasitic activity of ivermectin: four decades of research into a "wonder drug", Eur. J. Med. Chem. 261 (2023), 115838.
[4] A. Crump, S. Ōmura, Ivermectin, "Wonder drug" from Japan: the human use perspective, Proc. Jpn. Acad. B 87 (2011) 13–28.
[5] The 2015 Nobel Prize in Physiology or Medicine – Press release [on-line access: 2023–08–18], https://www.nobelprize.org/prizes/medicine/2015/press-release/..
[6] A. Markowska, J. Kaysiewicz, J. Markowska, A. Huczyński, Doxycycline, salinomycin, monensin and ivermectin repositioned as cancer drugs, Bioorg. Med. Chem. Lett. 29 (2019) 1549–1554.
[7] Ending the Neglect to Attain the Sustainable Development Goals: A Road Map for Neglected Tropical Diseases 2021–2030, World Health Organization, 2020.
[8] World Health Organization – Trypanosomiasis, Human African (Sleeping Sickness), [on-line access: 2023–09–15]..
[9] D. Malvy, F. Chappuis, Sleeping sickness, Clin. Microbiol. Infect. 17 (2011) 986–995.
[10] D. Steverding, Sleeping sickness and nagana disease caused by *Trypanosoma brucei*, in: Arthropod Borne Diseases, Springer International Publishing, 2017, pp. 277–297.
[11] P.H. Stoco, L.C. Miletti, K. Picozzi, M. Steindel, E.C. Grisard, Other major trypanosomiasis, in: Arthropod Borne Diseases, Springer International Publishing, Cham, 2017, pp. 299–324.
[12] N. Baker, H.P. de Koning, P. Mäser, D. Horn, Drug resistance in African trypanosomiasis: the melarsoprol and pentamidine story, Trends Parasitol. 29 (2013) 110–118.
[13] World Health Organization – Malaria, [on-line access: 2023–10–05]..
[14] M.A. Phillips, J.N. Burrows, C. Manyando, R.H. van Huijsduijnen, W.C. Van Voorhis, T.N.C. Wells, Malaria, Nat. Rev. Dis. Primers 3 (2017), 17050.
[15] M. Prudêncio, A. Rodriguez, M.M. Mota, The silent path to thousands of merozoites: the *Plasmodium* liver stage, Nat. Rev. Microbiol. 4 (2006) 849–856.
[16] Centers for Disease Control and Prevention – Malaria, [on-line access: 2023–09–15]..
[17] P.E. Duffy, J. Patrick Gorres, Malaria vaccines since 2000: progress, priorities, products, NPJ Vaccines 5 (2020) 48.
[18] N.J. White, Antimalarial drug resistance, J. Clin. Invest. 113 (2004) 1084–1092.
[19] S. Gupta, S. Vohra, K. Sethi, S. Gupta, B.C. Bera, S. Kumar, R. Kumar, *In vitro* anti-trypanosomal effect of ivermectin on *Trypanosoma evansi* by targeting multiple metabolic pathways, Trop. Anim. Health Prod. 54 (2022) 240.
[20] L. Fraccaroli, M.D. Ruiz, V.G. Perdomo, A.N. Clausi, D.E. Balcazar, L. Larocca, C. Carrillo, Broadening the spectrum of ivermectin: its effect on *Trypanosoma cruzi* and related trypanosomatids, Front. Cell. Infect. Microbiol. 12 (2022), 885268.
[21] U.K. Udensi, A.F. Fagbenro-Beyioku, Effect of ivermectin on *Trypanosoma brucei brucei* in experimentally infected mice, J. Vector Borne Dis. 49 (2012) 143–150.
[22] P.A. Langley, J.M. Roe, Ivermectin as a possible control agent for the tsetse fly, *Glossina morsitans*, Entomol. Exp. Appl. 36 (1984) 137–143.
[23] L. Singh, K. Singh, Ivermectin: a promising therapeutic for fighting malaria. Current status and perspective, J. Med. Chem. 64 (2021) 9711–9731.
[24] A.M. Mendes, I.S. Albuquerque, M. Machado, J. Pissarra, P. Meireles, M. Prudêncio, Inhibition of *Plasmodium* liver infection by ivermectin, Antimicrob. Agents Chemother. 61 (2017), e02005-e02016.
[25] T. Rodrigues, M. Prudêncio, R. Moreira, M.M. Mota, F. Lopes, Targeting the liver stage of malaria parasites: a yet unmet goal, J. Med. Chem. 55 (2012) 995–1012.
[26] S. Pampiglione, G. Majori, G. Petrangeli, R. Romi, Avermectins, MK-933 and MK-936, for mosquito control, Trans. R. Soc. Trop. Med. Hyg. 79 (1985) 797–799.
[27] L. Singh, D. Fontinha, D. Francisco, M. Prudêncio, K. Singh, Synthesis and antiplasmodial activity of regioisomers and epimers of second-generation dual acting ivermectin hybrids, Sci. Rep. 12 (2022) 564.
[28] L. Singh, D. Fontinha, D. Francisco, A.M. Mendes, M. Prudêncio, K. Singh, Molecular design and synthesis of ivermectin hybrids targeting hepatic and erythrocytic stages of *Plasmodium* parasites, J. Med. Chem. 63 (2020) 1750–1762.
[29] L. Dong, J. Zhang, Research progress of avermectin: a minireview based on the structural derivatization of avermectin, Adv. Agrochem. 1 (2022) 100–112.
[30] R.J. Cvetovich, D.H. Kelly, L.M. DiMichele, R.F. Shuman, E.J.J. Grabowski, Syntheses of 4″-*epi*-amino-4″-deoxyavermectins B1, J. Org. Chem. 59 (1994) 7704–7708.
[31] F. Ming-Kun, W. Xian, N. Jun, L. Jian-Zhong, Solid phase synthesis of 4″-*epi*-methylamino-4″-deoxyavermectin B1 benzoate, Chin, J. Chem. 23 (2005) 901–904.
[32] H. Mrozik, P. Eskola, B.H. Arison, B.O. Linn, A. Lusi, A. Matzuk, T.L. Shih, M. Tischler, F.S. Waksmunski, M.J. Wyvratt, T.A. Blizzard, G.M. Margiatto, M. H. Fisher, W.L. Shoop, J.R. Egerton, 4″-deoxy-4″-aminoavermectins with potent broad spectrum antiparasitic activities, Bioorg. Med. Chem. Lett. 5 (1995) 2435–2440.
[33] M.F. Loewe, R.J. Cvetovich, L.M. DiMichele, R.F. Shuman, E.J.J. Grabowski, Glycosidation route to 4″-*epi*-(methylamino)-4″-deoxyavermectin B1 (MK-244, emamectin benzoate), J. Org. Chem. 59 (1994) 7870–7875.
[34] G. Wei, Y. Du, R.J. Linhardt, New potent insecticidal agent: 4′-fucosyl avermectin derivative, Tetrahedron Lett. 45 (2004) 6895–6898.
[35] W.L. Shoop, H. Mrozik, M.H. Fisher, Structure and activity of avermectins and milbemycins in animal health, Vet. Parasitol. 59 (1995) 139–156.
[36] F. Huang, H. Ling, J. Li, S. Lu, W. Liu, Q. Li, F. Xu, Synthesis, bioactivities and 3D-QSAR of novel avermectin B2a aglycon derivatives, Chin. Chem. Lett. 31 (2020) 141–144.
[37] J.H. Zhao, X.J. Xu, M.H. Ji, J.L. Cheng, G.N. Zhu, Design, synthesis, and biological activities of milbemycin analogues, J. Agric. Food Chem. 59 (2011) 4836–4850.
[38] Milbemycins Analogues as Well as Preparation Method and Application Thereof in Pesticides, 2014 patent no. CN103936755A.
[39] H. Mrozik, B.O. Linn, P. Eskola, A. Lusi, A. Matzuk, F.A. Preiser, D.A. Ostlind, J. M. Schaeffer, M.H. Fisher, Syntheses and biological activities of 13-substituted avermectin aglycons, J. Med. Chem. 32 (1989) 375–381.
[40] B.R. Buckley, B. Fernández, D.-R., A catalytic, mild and efficient protocol for the C-3 aerial hydroxylation of oxindoles, Tetrahedron Lett. 54 (2013) 843–846.
[41] C.F. Macrae, I.J. Bruno, J.A. Chisholm, P.R. Edgington, P. McCabe, E. Pidcock, L. Rodriguez-Monge, R. Taylor, J. van de Streek, P.A. Wood, Mercury CSD 2.0 – new features for the visualization and investigation of crystal structures, J. Appl. Crystallogr. 41 (2008) 466–470.
[42] K. Shubin, A. Bērziņš, S. Belyakov, Crystal structures of new ivermectin pseudopolymorphs, Crystals 11 (2021) 172.
[43] J.P. Springer, B.H. Arison, J.M. Hirshfield, K. Hoogsteen, The absolute stereochemistry and conformation of avermectin B2a aglycone and avermectin B1a, J. Am. Chem. Soc. 103 (1981) 4221–4224.
[44] M. Antoszczak, K. Gadsby-Davis, D. Steverding, A. Huczyński, Synthesis of urea and thiourea derivatives of C20-*epi*-aminosalinomycin and their activity against *Trypanosoma brucei*, Eur. J. Med. Chem. 250 (2023), 115241.
[45] J.E. Huheey, The electronegativity of groups, J. Phys. Chem. 69 (1965) 3284–3291.
[46] M. Frigerio, M. Santagostino, S. Sputore, A user-friendly entry to 2-iodoxybenzoic acid (IBX), J. Org. Chem. 64 (1999) 4537–4538.
[47] G.M. Sheldrick, Crystal structure refinement with *SHELXL*, Acta Crystallogr. C Struct. Chem. 71 (2015) 3–8.
[48] G.M. Sheldrick, A short history of *SHELX*, Acta Crystallogr. A. 64 (2008) 112–122.
[49] O.V. Dolomanov, L.J. Bourhis, R.J. Gildea, J.A.K. Howard, H. Puschmann, *OLEX2* : a complete structure solution, refinement and analysis program, J. Appl. Crystallogr. 42 (2009) 339–341.
[50] C.F. Macrae, I. Sovago, S.J. Cottrell, P.T.A. Galek, P. McCabe, E. Pidcock, M. Platings, G.P. Shields, J.S. Stevens, M. Towler, P.A. Wood, Mercury 4.0: from visualization to analysis, design and prediction, J. Appl. Crystallogr. 53 (2020) 226–235.
[51] H. Hirumi, K. Hirumi, J.J. Doyle, G.A.M. Cross, *In vitro* cloning of animal-infective bloodstream forms of *Trypanosoma brucei*, Parasitology 80 (1980) 371–382.
[52] S.J. Collins, R.C. Gallo, R.E. Gallagher, Continuous growth and differentiation of human myeloid leukaemic cells in suspension culture, Nature 270 (1977) 347–349.
[53] T. Baltz, D. Baltz, C. Giroud, J. Crockett, Cultivation in a semi-defined medium of animal infective forms of Trypanosoma brucei, T. equiperdum, T. evansi, T. rhodesiense and T. gambiense, EMBO J. 4 (1985) 1273–1277.
[54] W. Huber, J.C. Koella, A comparison of three methods of estimating EC_{50} in studies of drug resistance of malaria parasites, Acta Trop. 55 (1993) 257–261.
[55] I.H.J. Ploemen, M. Prudêncio, B.G. Douradinha, J. Ramesar, J. Fonager, G.J. van Gemert, A.J.F. Luty, C.C. Hermsen, R.W. Sauerwein, F.G. Baptista, M.M. Mota, A. P. Waters, I. Que, C.W.G.M. Lowik, S.M. Khan, C.J. Janse, B.M.D. Franke-Fayard, Visualisation and quantitative analysis of the rodent malaria liver stage by real time imaging, PLoS One 4 (2009), e7881.